NASA Technical Memorandum 4138

Low-Speed Static and Dynamic Force Tests of a Generic Supersonic Cruise Fighter Configuration

David E. Hahne

OCTOBER 1989

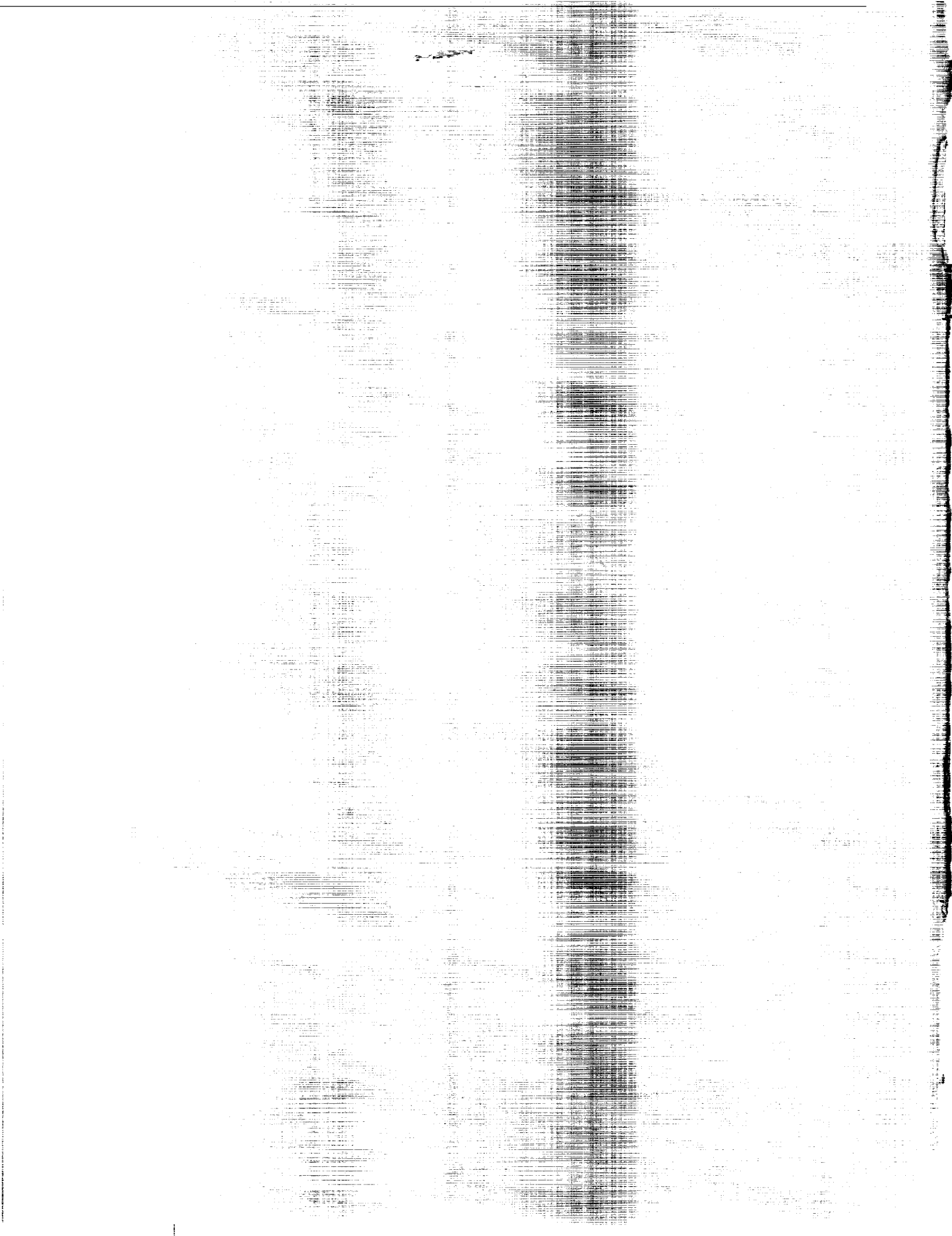

NASA Technical Memorandum 4138

Low-Speed Static and Dynamic Force Tests of a Generic Supersonic Cruise Fighter Configuration

David E. Hahne
Langley Research Center
Hampton, Virginia

National Aeronautics and
Space Administration
Office of Management
Scientific and Technical
Information Division

1989

Summary

Static and dynamic force tests of a generic fighter configuration designed for sustained supersonic flight have been conducted in the Langley 30- by 60-Foot Tunnel. The baseline configuration had a 65° arrow wing, twin vertical tails, and a canard. This configuration resulted from a series of studies conducted as part of a cooperative program between the NASA Langley Research Center and the McDonnell Aircraft Company to develop a low-speed design data base for supersonic cruise configurations.

The results of the investigation showed that the baseline configuration with a canard exhibited a pitch-up between angles of attack of 15° and 20°. Control was available up to $C_{L,\max}$ (maximum lift coefficient) from aerodynamic controls about all axes, but control in the pitch and yaw axes decreased rapidly in the poststall angle-of-attack region. The baseline configuration showed stable lateral-directional characteristics at low angles of attack, but directional instability occurred near an angle of attack of 25° as the wing shielded the vertical tails. The configuration showed positive effective dihedral throughout the test angle-of-attack range. Forced oscillation tests indicated that the baseline configuration had stable damping characteristics about the lateral-directional axes.

Introduction

Static and dynamic force tests of a generic fighter configuration designed for sustained supersonic flight have been conducted in the Langley 30- by 60-Foot Tunnel. These tests were undertaken to document the low-speed static and dynamic stability and control characteristics of a generic fighter configuration designed for sustained supersonic flight (fig. 1). This test configuration resulted from a series of studies conducted as part of a cooperative program between the NASA Langley Research Center and the McDonnell Aircraft Company to develop a low-speed design data base for supersonic cruise configurations (refs. 1, 2, and 3). These past investigations provided basic information for evaluation of a variety of forebody and vertical tail geometries as well as various conventional and advanced control concepts. A supersonic wing design study (ref. 3) and a sizing study similar to that described in reference 1 were also used in determining the test configurations.

This report presents results of both static and dynamic force tests for a variety of configuration variations. Both longitudinal and lateral-directional data were obtained during the static force tests. Lateral-directional data were obtained during dynamic force tests, and the results are presented herein.

Symbols

All data were initially obtained in the body-axis system (fig. 2). Longitudinal forces and moments are presented in the stability-axis system, and lateral-directional forces and moments are presented in the body-axis system. A moment reference center of $0.38\bar{c}$ was used for all tests.

b	wing span, ft
C_D	drag coefficient, $\frac{\text{Drag}}{\bar{q}S}$
C_L	lift coefficient, $\frac{\text{Lift}}{\bar{q}S}$
$C_{L,\max}$	maximum lift coefficient
C_l	rolling-moment coefficient, $\frac{\text{Rolling moment}}{\bar{q}Sb}$
C_m	pitching-moment coefficient, $\frac{\text{Pitching moment}}{\bar{q}S\bar{c}}$
C_n	yawing-moment coefficient, $\frac{\text{Yawing moment}}{\bar{q}Sb}$
C_Y	side-force coefficient, $\frac{\text{Side force}}{\bar{q}S}$
$\bar{c}$	mean aerodynamic chord, ft
f	frequency of oscillation, Hz
k	reduced-frequency parameter, $\frac{\omega b}{2V}$
p, q, r	angular velocity about X, Y, and Z body axes, rad/sec
$\bar{q}$	free-stream dynamic pressure, lb/ft
S	wing area, ft^2
u, v, w	linear velocity along X, Y, and Z body axes, respectively, ft/sec
V	free-stream velocity, ft/sec
X, Y, Z	body axes
α	angle of attack, deg
β	angle of sideslip, deg
$\dot{\beta}$	rate of change of sideslip, rad/sec
ΔC_l	incremental rolling-moment coefficient
ΔC_n	incremental yawing-moment coefficient
ΔC_Y	incremental side-force coefficient

δ_a	aileron deflection, positive for right trailing edge down, left trailing edge up, deg
δ_c	canard deflection, positive for trailing edge down, deg
δ_F	flap deflection, wing trailing-edge extension, positive for trailing edge down, deg
δ_f	leading-edge flap deflection, positive for leading edge down, deg
δ_r	rudder deflection, positive for trailing edge left, deg
δ_{wt}	wingtip deflection, positive for right trailing edge down, left trailing edge up, deg
ω	angular velocity, $2\pi f$, rad/sec

Stability derivatives:

$$C_{l_p} = \frac{\partial C_l}{\partial \frac{pb}{2V}} \quad C_{l_r} = \frac{\partial C_l}{\partial \frac{rb}{2V}} \quad C_{l_\beta} = \frac{\partial C_l}{\partial \beta} \quad C_{l_{\dot\beta}} = \frac{\partial C_l}{\partial \frac{\dot\beta b}{2V}}$$

$$C_{n_p} = \frac{\partial C_n}{\partial \frac{pb}{2V}} \quad C_{n_r} = \frac{\partial C_n}{\partial \frac{rb}{2V}} \quad C_{n_\beta} = \frac{\partial C_n}{\partial \beta} \quad C_{n_{\dot\beta}} = \frac{\partial C_n}{\partial \frac{\dot\beta b}{2V}}$$

$$C_{Y_p} = \frac{\partial C_Y}{\partial \frac{pb}{2V}} \quad C_{Y_r} = \frac{\partial C_Y}{\partial \frac{rb}{2V}} \quad C_{Y_\beta} = \frac{\partial C_Y}{\partial \beta} \quad C_{Y_{\dot\beta}} = \frac{\partial C_Y}{\partial \frac{\dot\beta b}{2V}}$$

Abbreviations:

B	body
BL	butt line
C	canard
cg	center of gravity
LE	leading edge
MS	model station
TEX	trailing-edge extension
V	vertical tails
W	wing
Y	wing trailing-edge extension

Model

Tests were made with a 0.14-scale model (fig. 1) in the Langley 30- by 60-Foot Tunnel. A sketch of the baseline configuration and details of the wing, canard, vertical tails, and control surfaces can be found in figure 3. Geometric characteristics can be found in table I. The model had an arrow wing with a 65° swept leading edge and an aspect ratio of 1.95. A close-coupled canard was mounted just above the engine inlets. Deflectable surfaces on the wing included a leading-edge flap, ailerons, and tiperons (deflectable wingtips). A flap at the end of the trailing-edge extension (TEX), which is similar to the fuselage strake found on the X-29A (see ref. 4), was used for pitch control in addition to the canard. Twin vertical tails mounted on the trailing-edge extension were canted inboard 15°. Conventional rudders were incorporated on the vertical tails. Angular deflections of all moving surfaces were measured perpendicular to the hinge line, and the range of deflections are given in table II.

Tests and Apparatus

All tests were conducted in the Langley 30- by 60-Foot Tunnel at a free-stream dynamic pressure of 10 psf, which corresponds to a Reynolds number of 1.89×10^6 based on the wing mean aerodynamic chord (fig. 4). Aerodynamic force and moment data were measured with a six-component strain-gage balance. Static data were obtained over a range of angle of attack from 0° to 65° at angles of sideslip of 0° and ±5° for a moment reference center of $0.38\bar{c}$. No corrections for base drag were made to the data, and because of the large test section no corrections for wall effects were needed. Flow angularity corrections were made for both angle of attack and angle of sideslip. The test setup for both roll and yaw forced oscillation tests is shown in figure 5. All forced oscillation data shown in this report were obtained at an amplitude of ±5° and a frequency of 0.75 Hz. This frequency resulted in a reduced-frequency parameter (k) value of 0.13. Further details of the forced oscillation technique can be found in reference 5.

Results and Discussion

Static Longitudinal Characteristics

Static longitudinal characteristics are presented in figures 6 through 10. The baseline configuration, with the canard set at a nominal deflection of −10°, was approximately 6 percent unstable at low angles of attack (fig. 6). The wing/body configuration was slightly longitudinally unstable for the chosen reference cg location. The addition of the wing TEX resulted in a configuration that is slightly stable at low angles of attack, with an increase in stability above $\alpha = 15°$. The relatively large difference seen in lift coefficient with the addition of the TEX is because the total wing reference area (wing plus wing TEX) was used in reducing all the data. The addition of the vertical tails to the configuration caused a large

decrease in lift. A similar result was seen in the tests of the model of reference 2 and is believed to be caused by interference of the vertical tails with the wing vortex system. This interference also results in a pitch-up at $\alpha = 15°$. The effect of leading-edge flap deflection is shown in figure 7. The data show that deflecting the leading-edge flap reduces the severity of the pitch-up that occurs near $\alpha = 15°$. With the leading-edge flap deflected 30°, the model showed much less pitch-up than with the flap undeflected. Because of the more desirable pitching-moment characteristic associated with this leading-edge deflection, the leading-edge flap was deflected 30° for most of the test.

Pitch control effectiveness of the canard and the TEX flaps is shown in figures 8 and 9, respectively. The data of figure 8 show that the canard is effective for pitch control and that the canard can be used for pitch trim up to $C_{L,\max}$ ($\alpha = 40°$). The effect of canard deflection on lift is small for moderate canard deflections. The negative lift generated by the canard deflected $-40°$ results in a noticeable reduction in lift up to $C_{L,\max}$. The reduction in lift near $C_{L,\max}$ for the canard deflected 20° is either the result of canard stall or the effect of the canard downwash on the wing or possibly both. The data of figure 9 show that the TEX flaps are slightly more powerful for pitch control than the canard, although the maximum C_L trim capability is similar for both controls. As expected, the combination of the canard and the TEX flaps for pitch control (fig. 10) provides increased pitch control up to $C_{L,\max}$.

Static Lateral-Directional Stability

The static lateral-directional stability characteristics for the configuration buildup are shown in figure 11. The baseline configuration showed static directional stability (positive values of C_{n_β}) at low angles of attack but became directionally unstable well before $C_{L,\max}$. The wing/body configuration was directionally unstable at low and moderate angles of attack but became directionally stable in the poststall region. Previous tests (ref. 6) indicated that the high-angle-of-attack stability shown in figure 11 is dependent on the forebody cross-sectional shape. The vertical tails generally provided a positive increment to C_{n_β} to angles of attack just past $C_{L,\max}$, even though the configuration initially lost directional stability near $\alpha = 20°$. At angles of attack beyond $\alpha = 45°$, the vertical tails were destabilizing directionally. As can be seen from figure 11, the canard degraded directional stability over most of the test angle-of-attack range. The canard, however, did improve directional stability slightly between angles of attack of 20° and 25° by delaying directional instability about 3° over the canard-off (BWYV) configuration. Laterally, the baseline configuration was stable throughout the test angle-of-attack range (negative values of C_{l_β}). Lateral stability of the wing/body configuration was typical for highly swept wing configurations. That is, the lateral stability increased with increasing angle of attack with an unstable break near $C_{L,\max}$. This unstable break has been shown from past research (ref. 7) to be a result of the asymmetric bursting of the wing vortex system. The addition of the wing TEX delays the unstable break in C_{l_β}, but the lateral instability is much more severe at higher angles of attack. The addition of the vertical tails forces the wing vortices to burst more symmetrically, thus eliminating the lateral instability. As can be seen, the canard further enhanced the lateral stability of the configuration.

The effect of leading-edge flap deflection on the lateral-directional characteristics of the baseline configuration is shown in figure 12. Increasing the leading-edge flap deflection had very little effect on the lateral-directional stability characteristics, although a slight increase in directional stability with increasing flap deflection can be seen around $\alpha = 20°$.

The data of figure 13 show that canard deflection had some influence on the lateral-directional characteristics for the baseline configuration. As might be expected, the larger canard deflections produced the greatest effects. With a canard deflection of $-40°$, directional instability occurred by $\alpha = 20°$. Lateral stability was also affected by canard deflection, although the effect was predominantly at the lower angles of attack. A canard deflection of $-40°$ caused a break in lateral stability at $\alpha = 8°$, whereas a 20° canard deflection had the effect of delaying the break in lateral stability to $\alpha = 20°$.

Lateral-Directional Control Characteristics

Control effectiveness for the aileron, tiperons, and rudders is shown in figures 14 through 17. The data of figure 14 show that the ailerons are effective for roll control at low angles of attack but that the effectiveness starts to decrease past $\alpha = 20°$. The data of figure 15 show that the tiperons are effective for roll control at low angles of attack and that some effectiveness is maintained throughout the test angle-of-attack range. The low-α effectiveness of the tiperons is comparable to that of the ailerons (fig. 16); however, past $\alpha = 20°$ aileron effectiveness is considerably less than that of the tiperons. The combination of the two surfaces provides for good levels of roll control past $C_{L,\max}$. It can also be seen in figure 16 that the tiperons generate smaller yawing moments than those produced by the ailerons.

However, the combination of ailerons and tiperons produces yawing moments similar to those produced by the ailerons alone. Rudder effectiveness for 10° rudder deflection (fig. 17) remains nearly constant up to $C_{L,\max}$, but the rudder effectiveness decreases rapidly beyond $\alpha = 40°$. For a rudder deflection of 30°, rudder authority tends to decrease with increasing angle of attack and becomes ineffective near $\alpha = 50°$.

Lateral-Directional Damping Characteristics

The results of the forced oscillation tests are shown in figures 18 through 25. Stable values of roll damping ($C_{l_p} - C_{l_{\dot{\beta}}} \cos\alpha$) and yaw damping ($C_{n_r} - C_{n_{\dot{\beta}}} \cos\alpha$) are negative. The data of figure 18 show that the addition of the vertical tails greatly decreased the roll damping in the angle-of-attack range from 30° to 50°. The yaw damping data of figure 22 show that the addition of the vertical tails provided increased yaw damping, as expected, but $C_{l_r} - C_{l_{\dot{\beta}}} \cos\alpha$ showed large reductions in the angle-of-attack range from 30° to 50°. The large reduction in the roll damping and $C_{l_r} - C_{l_{\dot{\beta}}} \cos\alpha$ is believed to be associated with the influence of the vertical tails on wing vortex breakdown, as discussed earlier in the static lateral-directional stability section of this report.

The data of figures 19 and 23 show that the effects of leading-edge flap deflection were small on roll damping and yaw damping. The effects of TEX flap deflection (figs. 20 and 24) were more pronounced on $C_{n_p} + C_{n_{\dot{\beta}}} \sin\alpha$ near $C_{L,\max}$. Figure 24 shows that yaw damping characteristics were increased with positive TEX flap deflection, while changes in $C_{l_r} - C_{l_{\dot{\beta}}} \cos\alpha$ were relatively small.

The data of figure 21 show that canard deflections had little effect on roll damping characteristics except for $\delta_c = -40°$, which decreased roll damping to zero near $\alpha = 30°$. Canard deflection had a much more pronounced effect on yaw damping (fig. 25) near $\alpha = 40°$, where damping varies from zero to large negative values as δ_c was changed from $-40°$ to 20°. Large changes in the side force and rolling moment due to yawing velocity were also noted near $\alpha = 40°$.

Summary of Results

The results of this investigation to document the static and dynamic stability and control characteristics of a generic supersonic cruise fighter configuration can be summarized as follows:

1. The baseline configuration was approximately 6 percent longitudinally unstable at low angles of attack and exhibited a pitch-up between angles of attack of 15° and 20°. The vertical tails increased the severity of the pitch-up and also caused a significant loss in lift compared with the tail-off configuration.
2. Pitch control was available up to $C_{L,\max}$ (maximum lift coefficient) from aerodynamic controls but decreased rapidly in the poststall angle-of-attack region.
3. The baseline configuration was directionally stable at low angles of attack but became directionally unstable near an angle of attack of 20° as the wing shielded the vertical tails. Static lateral stability was maintained throughout the test angle-of-attack range.
4. The combination of tiperons and ailerons provided roll control up to $C_{L,\max}$. Rudder power decreased with increasing angle of attack and became ineffective in the poststall region.
5. Forced oscillation tests indicated that the baseline configuration had stable lateral-directional damping characteristics up to $C_{L,\max}$.

NASA Langley Research Center
Hampton, VA 23665-5225
August 17, 1989

References

1. Wood, Richard M.; Miller, David S.; Hahne, David E.; Niedling, Larry G.; and Klein, John R.: Status Review of a Supersonically-Biased Fighter Wing-Design Study. AIAA-83-1857, July 1983.
2. Hahne, David E.: *Low-Speed Aerodynamic Stability and Control Characteristics of an Advanced Fighter Aircraft at High Angles of Attack.* NASA TP-2617, 1986.
3. Wood, Richard M.; and Miller, David S.: *Wing Planform Effects at Supersonic Speeds for an Advanced Fighter Configuration.* NASA TP-2269, 1984.
4. Murri, Daniel G.; Nguyen, Luat T.; and Grafton, Sue B.: *Wind-Tunnel Free-Flight Investigation of a Model of a Forward-Swept-Wing Fighter Configuration.* NASA TP-2230, 1984.
5. Grafton, Sue B.; and Libbey, Charles E.: *Dynamic Stability Derivatives of a Twin-Jet Fighter Model for Angles of Attack From −10° to 110°.* NASA TN D-6091, 1971.
6. Klein, John R.; Walck, Kenneth J.; and Hahne, David E.: Airframe Component Effects on the Aerodynamic Stability and Control Characteristics of a Supersonic Cruise Fighter Aircraft at High Angles of Attack. AIAA-84-2110, Aug. 1984.
7. Wentz, William H., Jr.; and Kohlman, David L.: *Wind Tunnel Investigations of Vortex Breakdown on Slender Sharp-Edged Wings.* NASA CR-98737, 1968.

Table I. Geometric Characteristics of Model

Overall fuselage length, ft	9.38
Wing:	
Airfoil section	NACA 64A004
Span, ft	5.14
Area, ft^2	13.56
Mean aerodynamic chord, ft	3.22
Aspect ratio	1.95
Leading-edge sweep, deg	65
Aileron area (one side), ft^2	0.30
Tiperon area (one side), ft^2	0.29
Vertical tails:	
Airfoil section (root)	NACA 65A005
Airfoil section (tip)	NACA 65A003
Area (each), ft^2	1.56
Span, ft	1.29
Root chord, ft	1.96
Tip chord, ft	0.45
Aspect ratio	1.07
Leading-edge sweep, deg	62.8
Rudder area (each), ft^2	0.29
Trailing-edge extension:	
Length, ft	2.2
Width, ft	0.65
Flap area (each), ft^2	0.45
Canard:	
Airfoil section (root)	5-percent biconvex
Airfoil section (tip)	3-percent biconvex
Area, ft^2	1.36
Span, ft	1.84
Tip chord, ft	0.30
Aspect ratio	2.48
Leading-edge sweep, deg	50

Table II. Deflection Range of Moving Surfaces

Surface	Deflection range, deg
LE flaps	0 to 30
Ailerons	±20
Tiperons	±40
TEX flaps	±30
Rudders	±30
Canard	−40 to 20

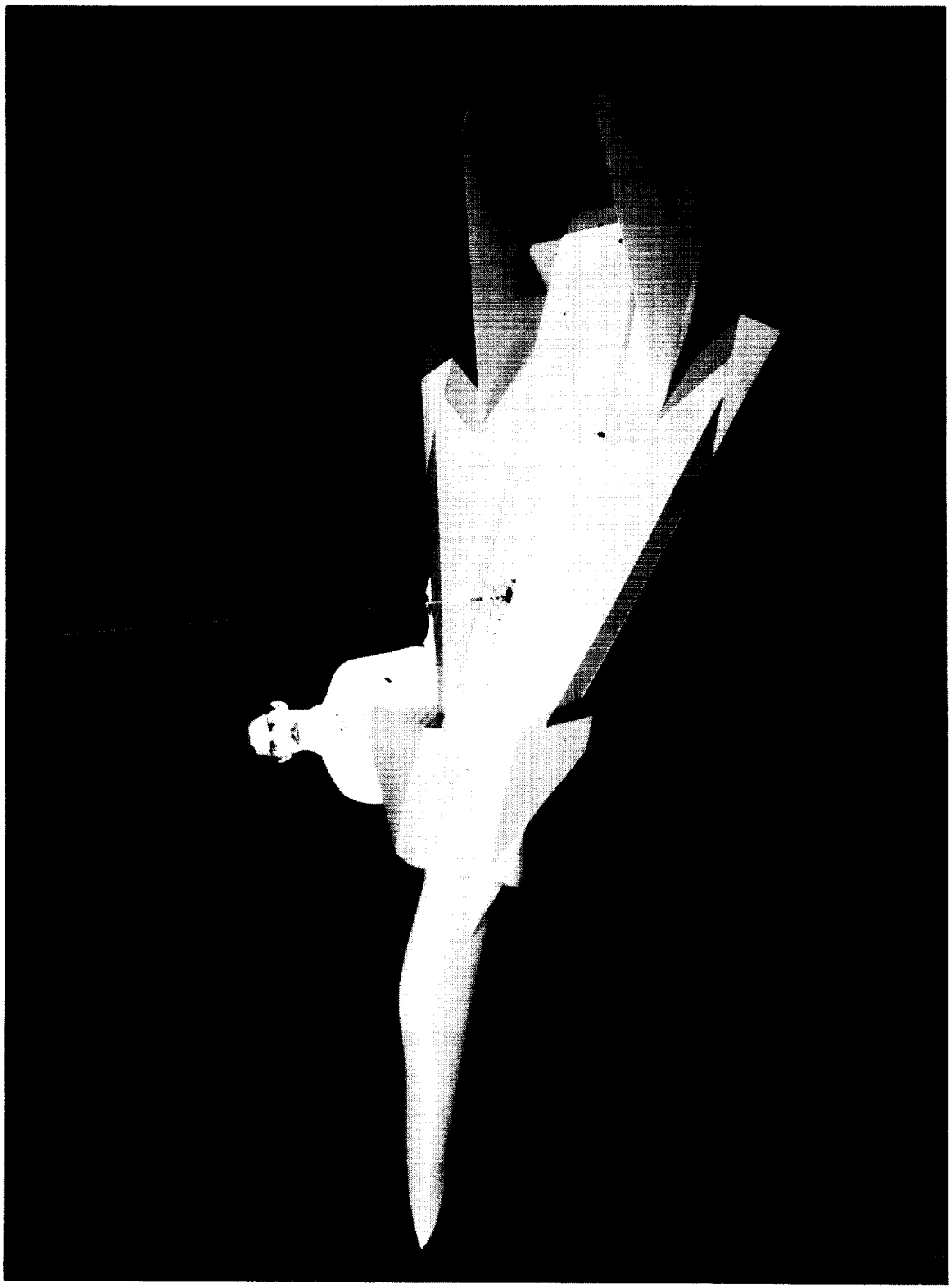

L-89-02517

Figure 1. Photograph of model.

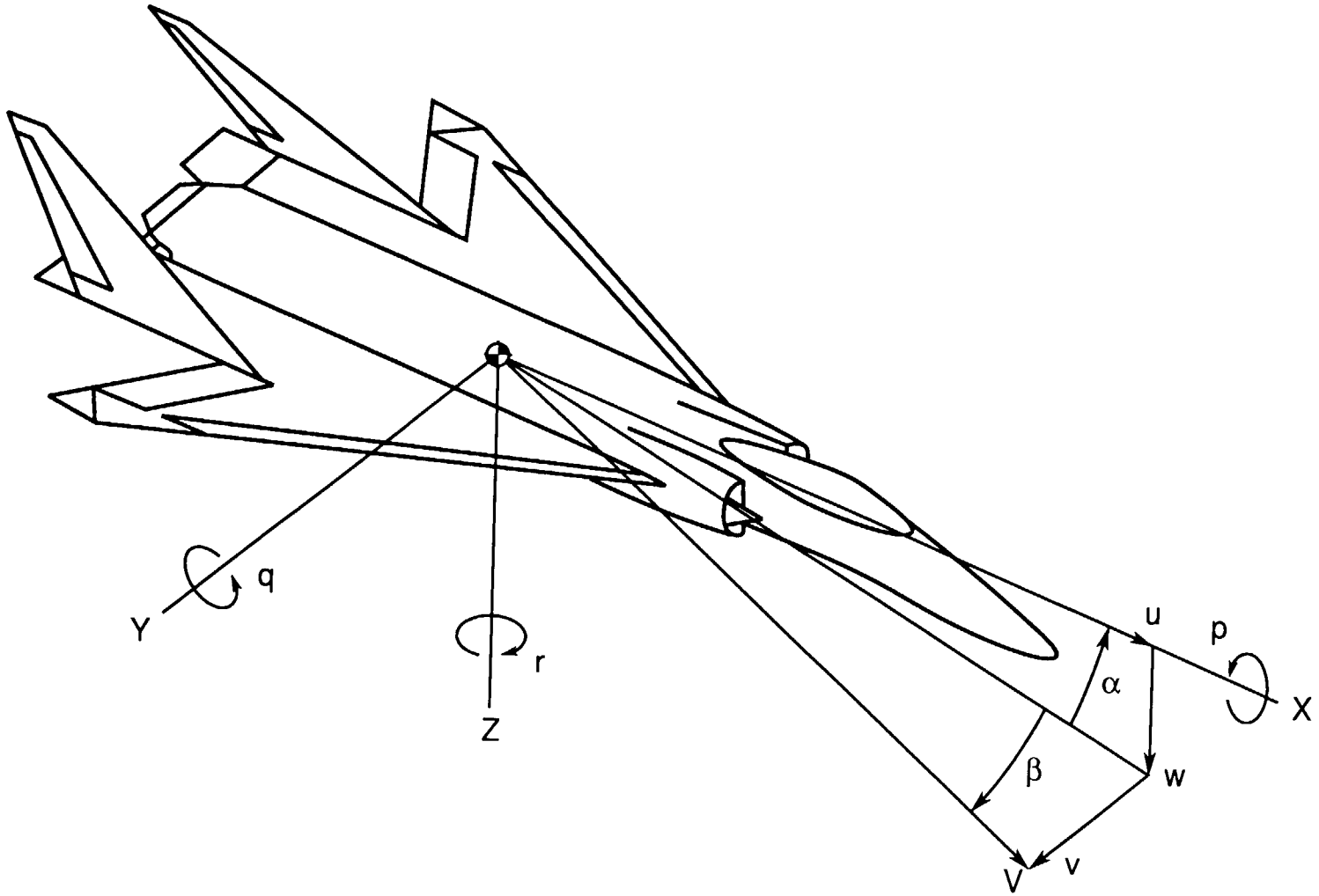

Figure 2. Definition of body-axis system.

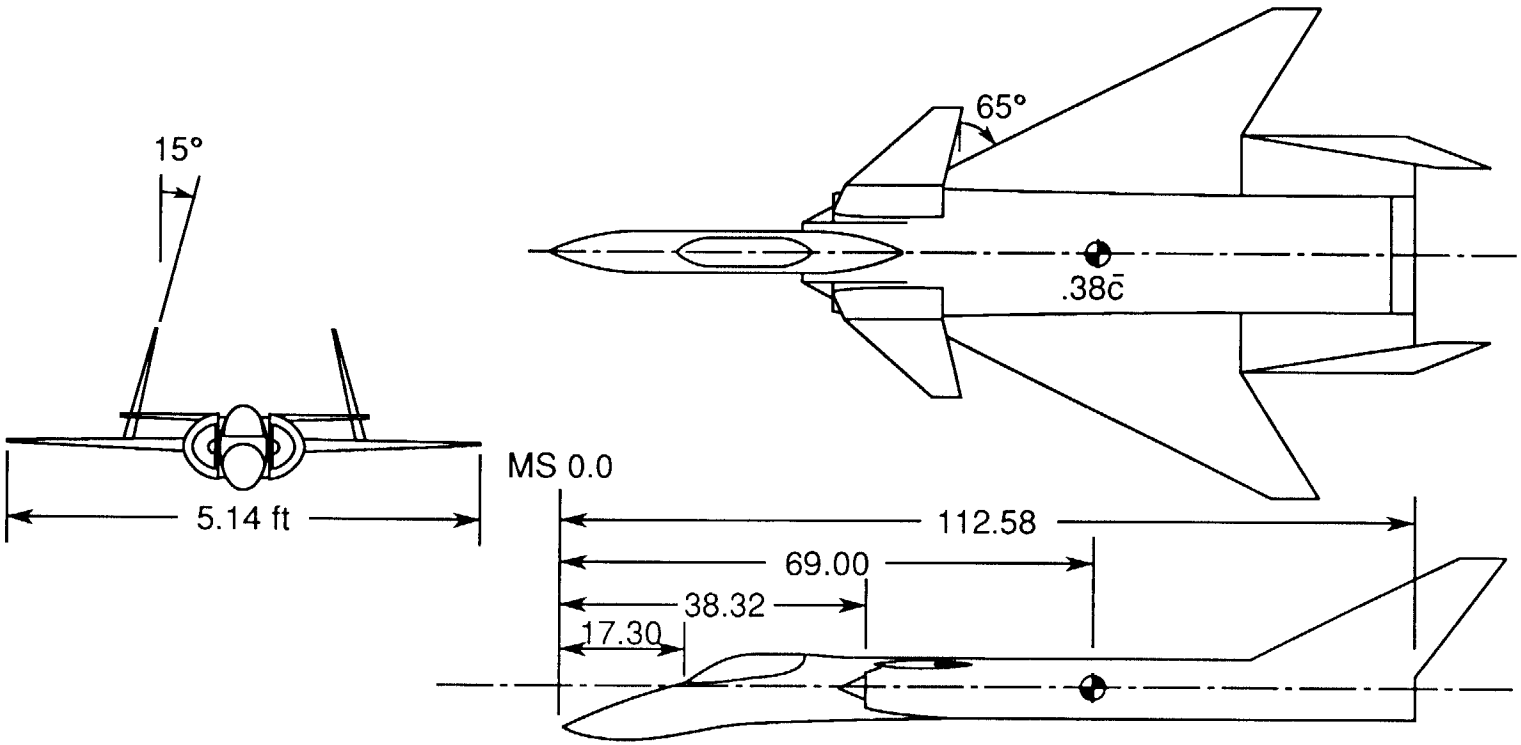

(a) Three-view sketch of model.

Figure 3. Details of baseline model geometry. Dimensions in inches except where noted.

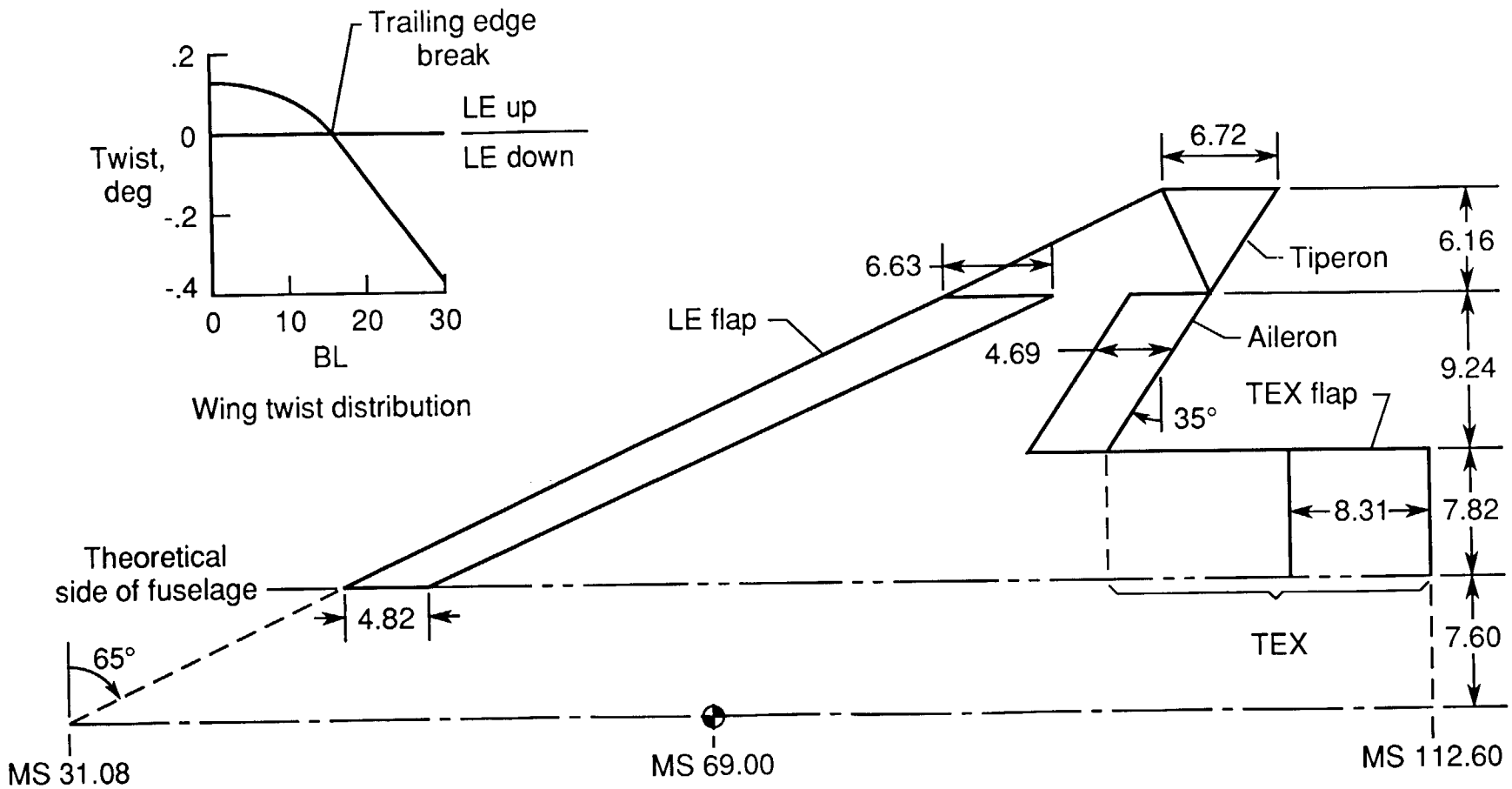

(b) Wing and TEX geometry; NACA 64A004 airfoil.

Figure 3. Continued.

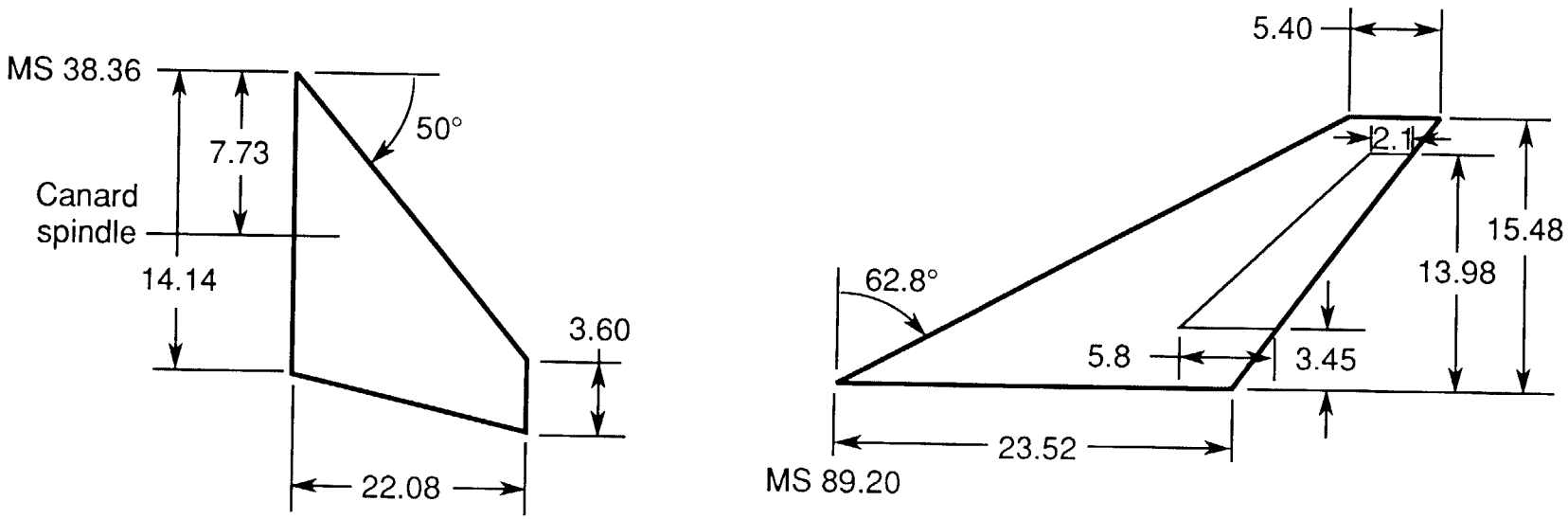

(c) Canard and vertical tail geometry.

Figure 3. Concluded.

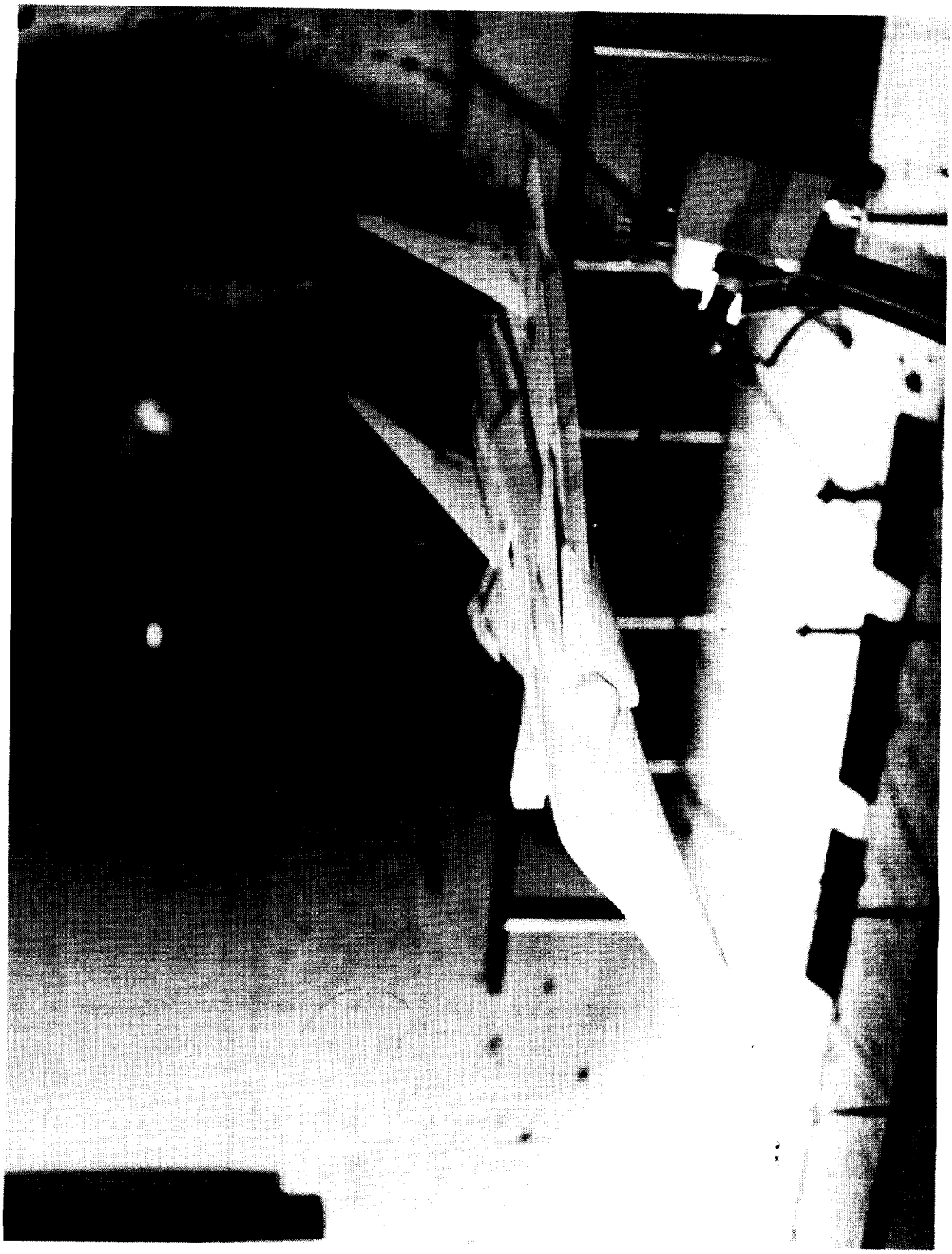

L-89-739

Figure 4. Model mounted in 30- by 60-Foot Tunnel.

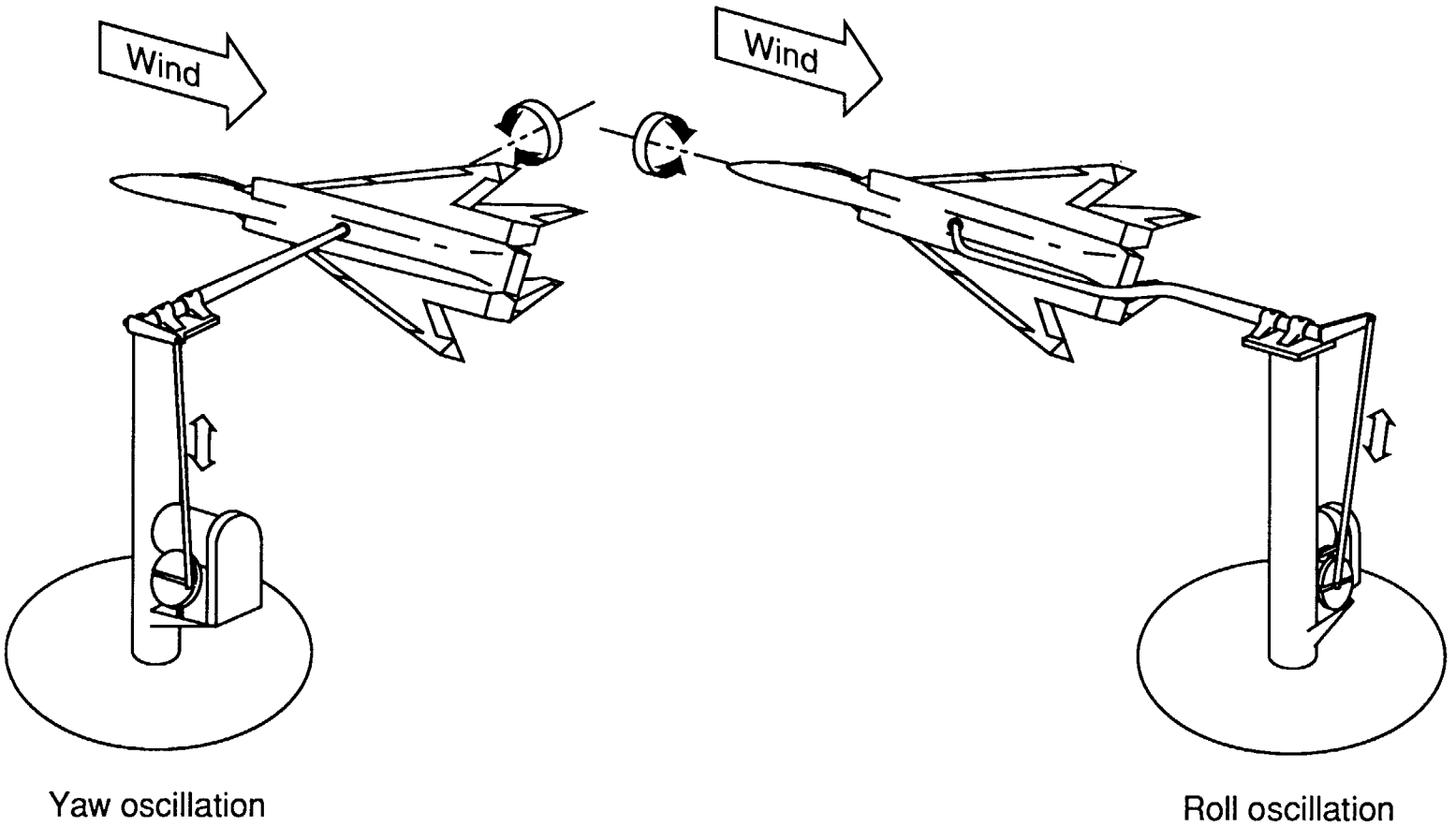

Figure 5. Sketch of yaw and roll oscillation test setups.

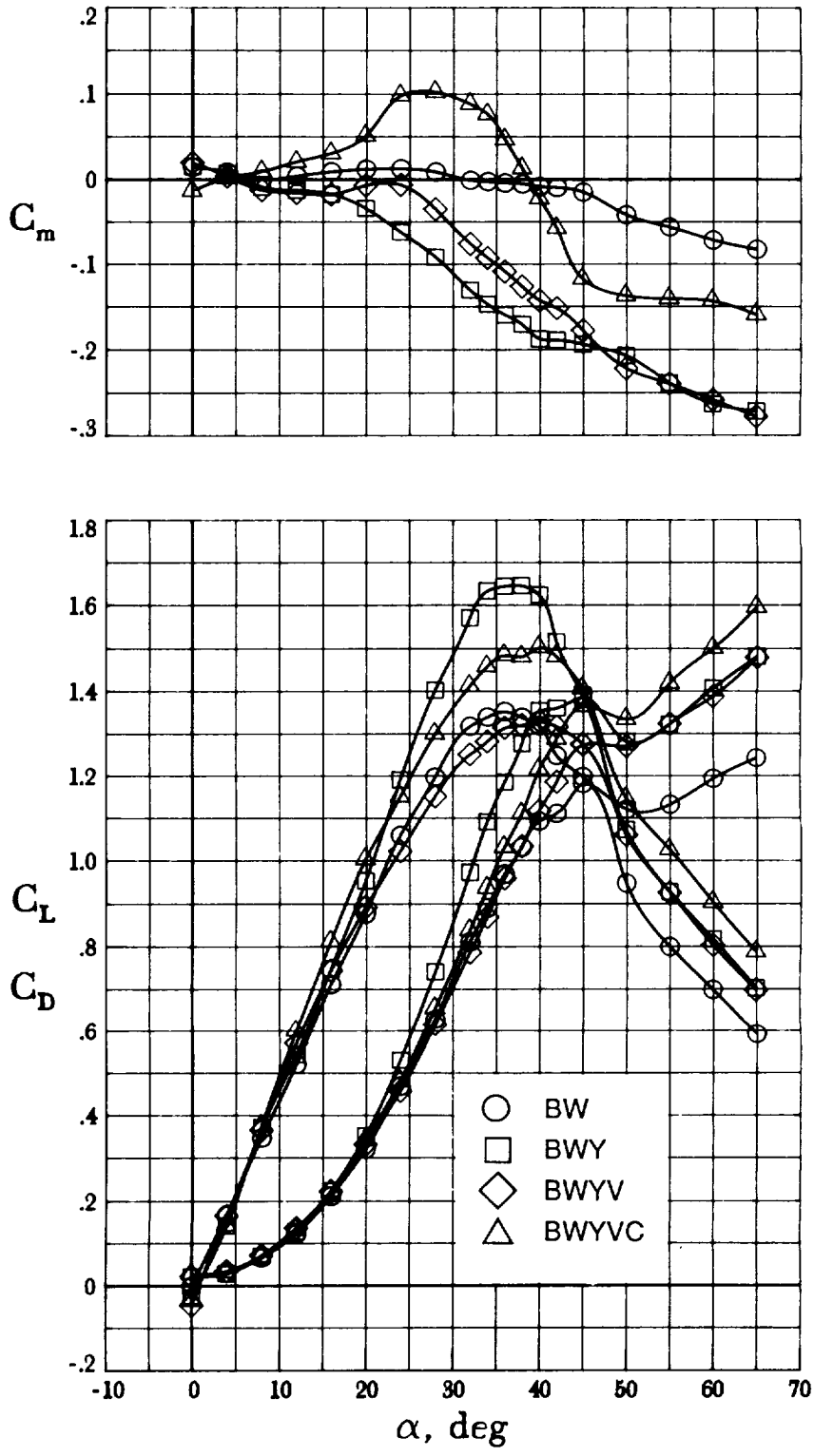

Figure 6. Effect of major geometry components on longitudinal characteristics. $\delta_f = 0°$; $\delta_c = -10°$; $\delta_F = 0°$.

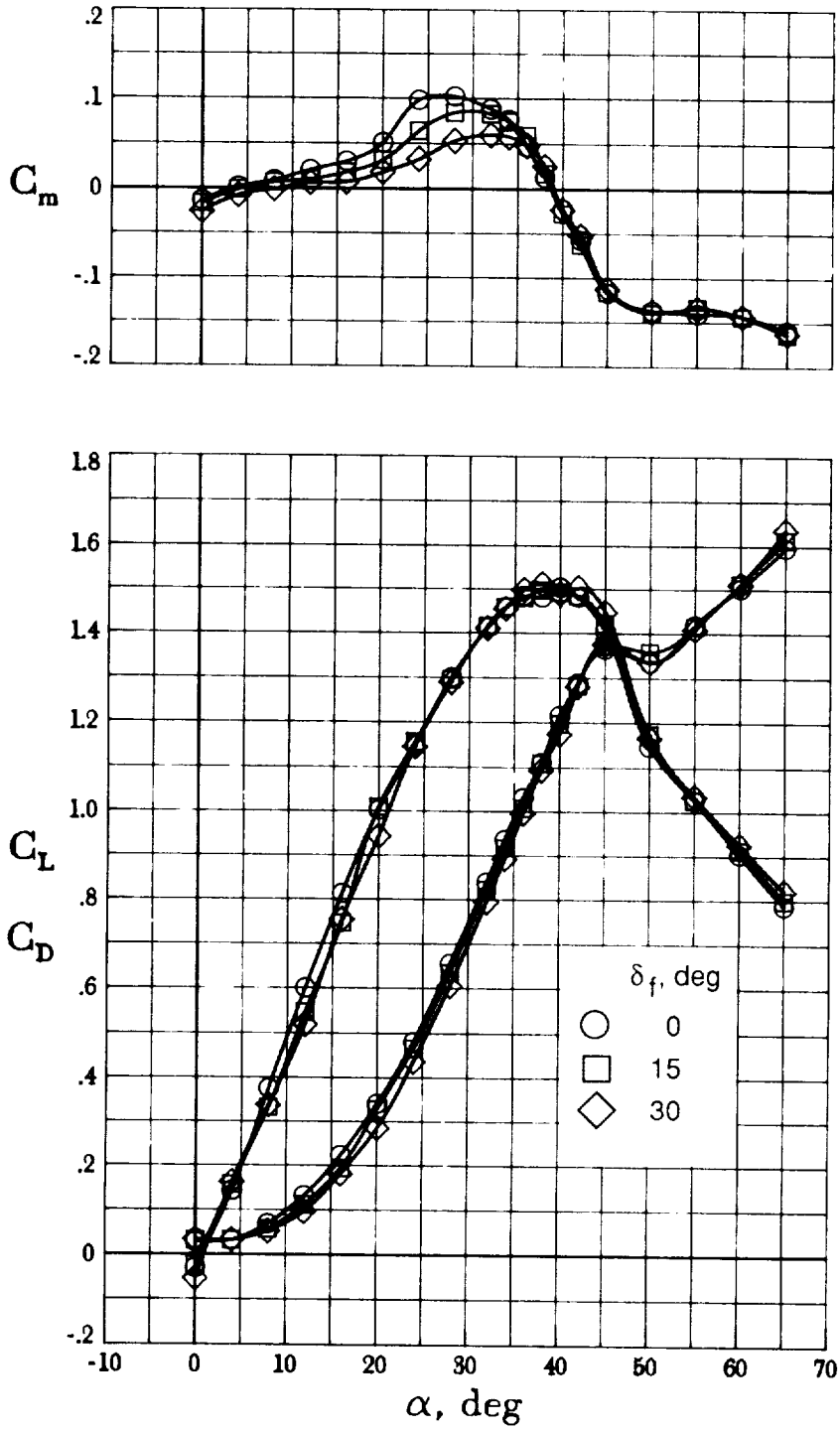

Figure 7. Effect of leading-edge flap deflection on longitudinal characteristics. $\delta_c = -10°$; $\delta_F = 0°$.

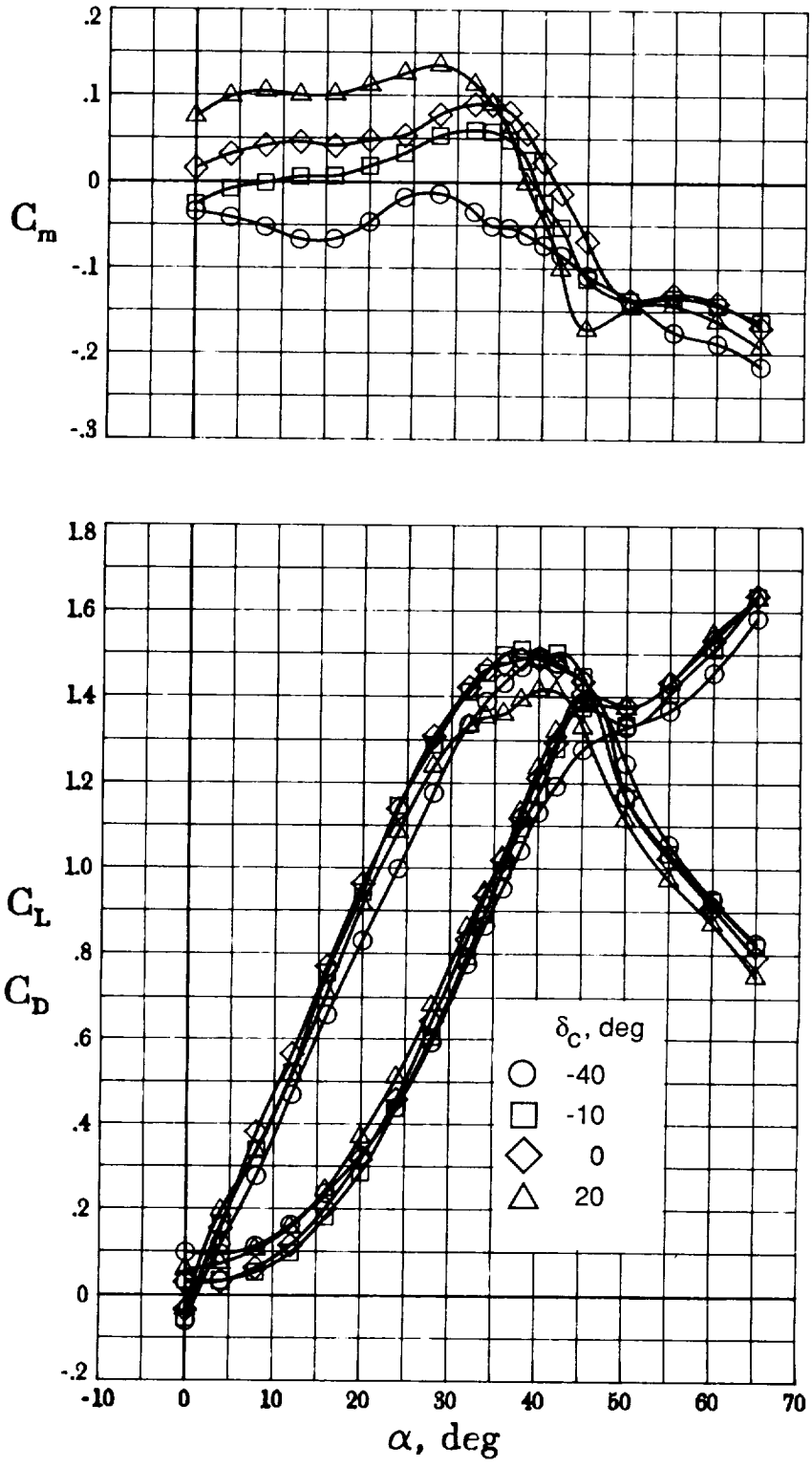

Figure 8. Effect of canard deflection on longitudinal characteristics. $\delta_f = 30°$; $\delta_F = 0°$.

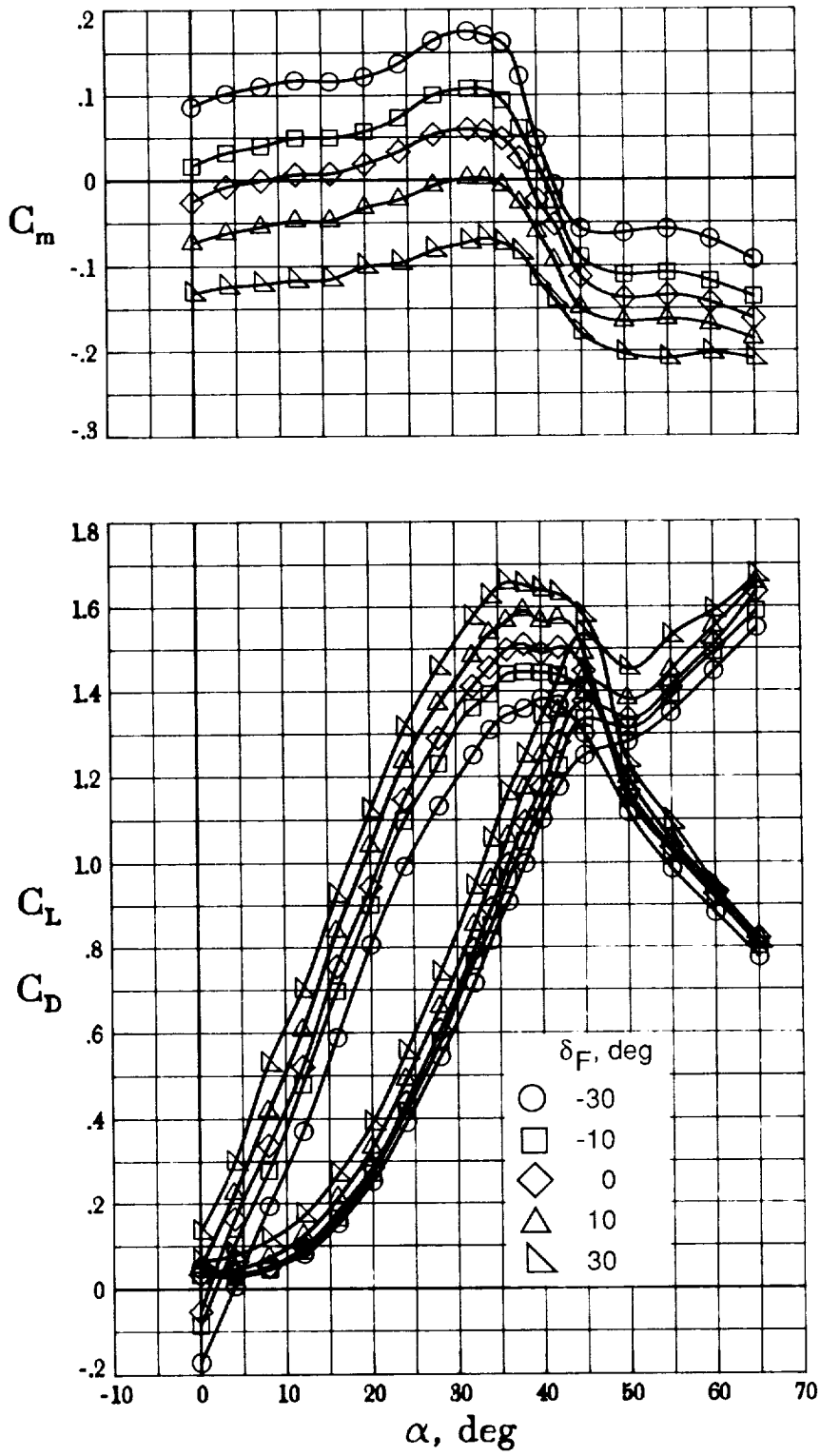

Figure 9. Effect of TEX flap deflection on longitudinal characteristics. $\delta_f = 30°$; $\delta_c = -10°$.

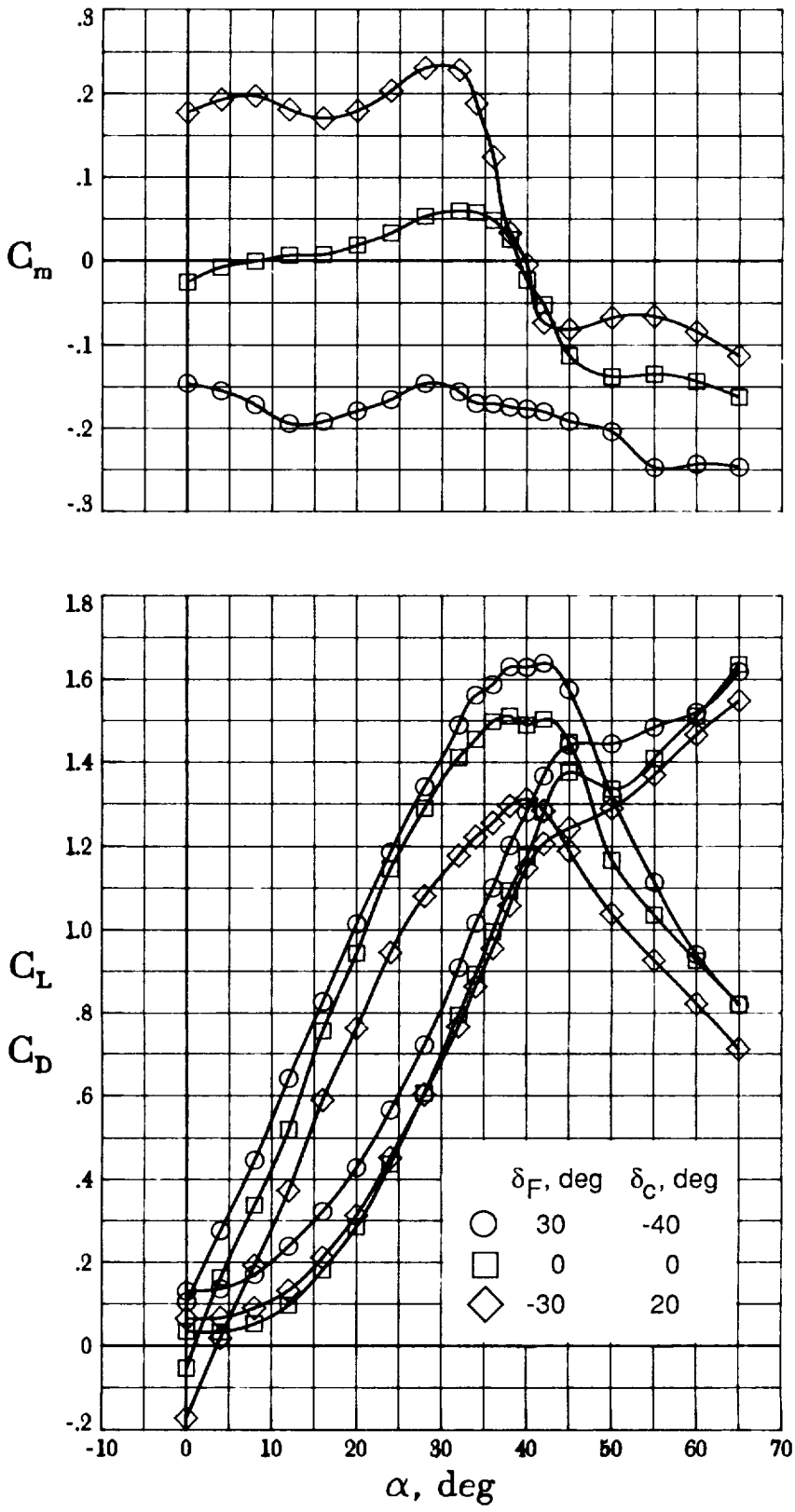

Figure 10. Combined pitch control characteristics. $\delta_f = 30°$.

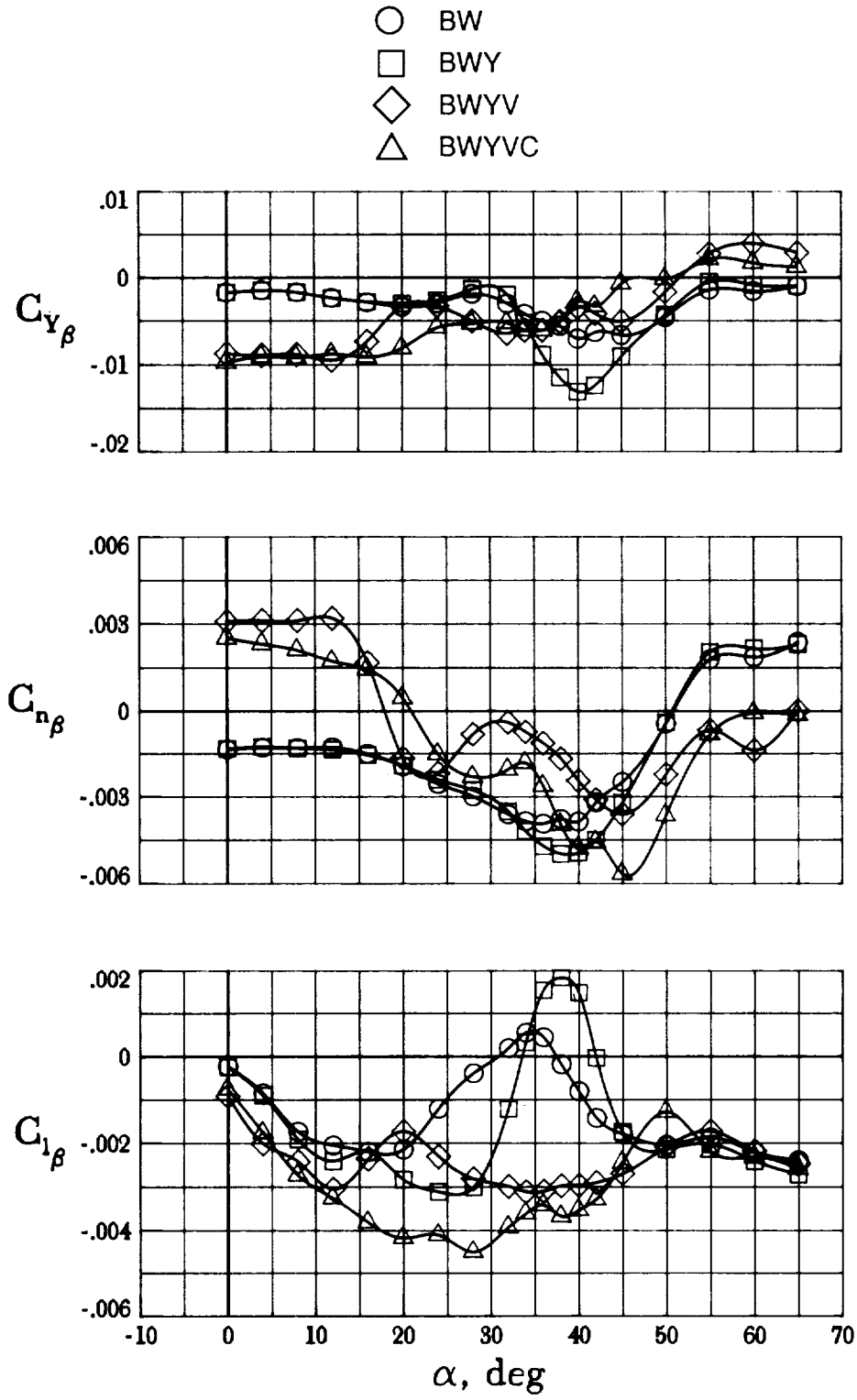

Figure 11. Effect of major geometry components on lateral-directional characteristics. $\delta_f = 0°$; $\delta_c = -10°$; $\delta_F = 0°$.

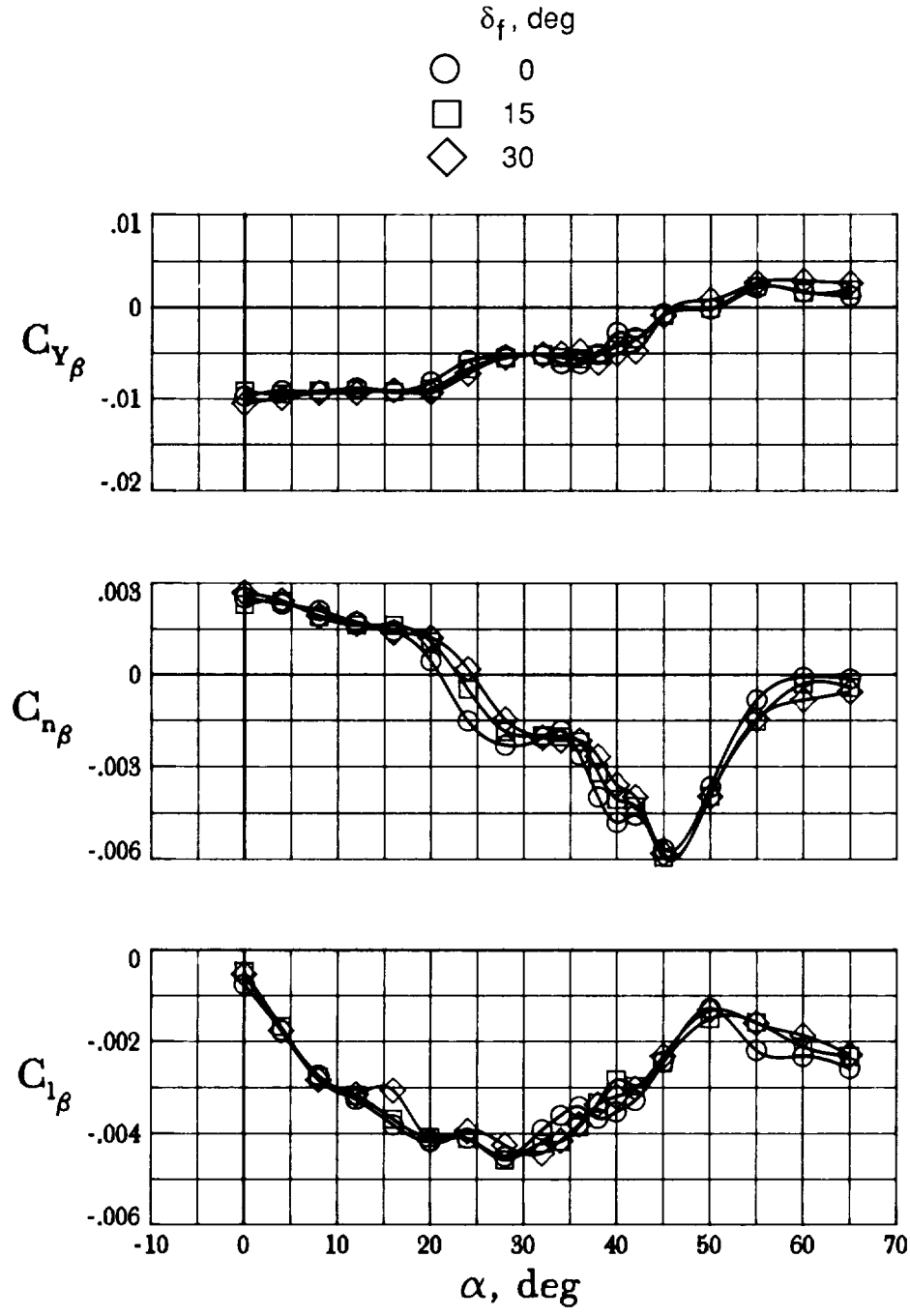

Figure 12. Effect of leading-edge flap deflection on lateral-directional characteristics. $\delta_c = -10°$; $\delta_F = 0°$.

NASA
National Aeronautics and Space Administration

Report Documentation Page

1. Report No.	2. Government Accession No.	3. Recipient's Catalog No.
NASA TM-4138		

4. Title and Subtitle	5. Report Date
Low-Speed Static and Dynamic Force Tests of a Generic Supersonic Cruise Fighter Configuration	October 1989
	6. Performing Organization Code
7. Author(s)	8. Performing Organization Report No.
David E. Hahne	L-16599
9. Performing Organization Name and Address	10. Work Unit No.
NASA Langley Research Center Hampton, VA 23665-5225	505-61-71-07
	11. Contract or Grant No.
12. Sponsoring Agency Name and Address	13. Type of Report and Period Covered
National Aeronautics and Space Administration Washington, DC 20546-0001	Technical Memorandum
	14. Sponsoring Agency Code

15. Supplementary Notes

16. Abstract

Static and dynamic force tests of a generic fighter configuration designed for sustained supersonic flight have been conducted in the Langley 30- by 60-Foot Tunnel. The baseline configuration had a 65° arrow wing, twin vertical tails, and a canard. The results of the investigation showed that control was available up to $C_{L,\max}$ (maximum lift coefficient) from aerodynamic controls about all axes, but control in the pitch and yaw angles decreased rapidly in the poststall angle-of-attack region. The baseline configuration showed stable lateral-directional characteristics at low angles of attack but directional stability occurred near an angle of attack of 25° as the wing shielded the vertical tails. The configuration showed positive effective dihedral throughout the test angle-of-attack range. Forced oscillation tests indicated that the baseline configuration had stable damping characteristics about the lateral-directional axes.

17. Key Words (Suggested by Authors(s))	18. Distribution Statement
Stability and control Aerodynamic control concepts Dynamic stability Arrow wing	Unclassified—Unlimited Subject Category 02

19. Security Classif. (of this report)	20. Security Classif. (of this page)	21. No. of Pages	22. Price
Unclassified	Unclassified	33	A03

For sale by the National Technical Information Service, Springfield, Virginia 22161-2171

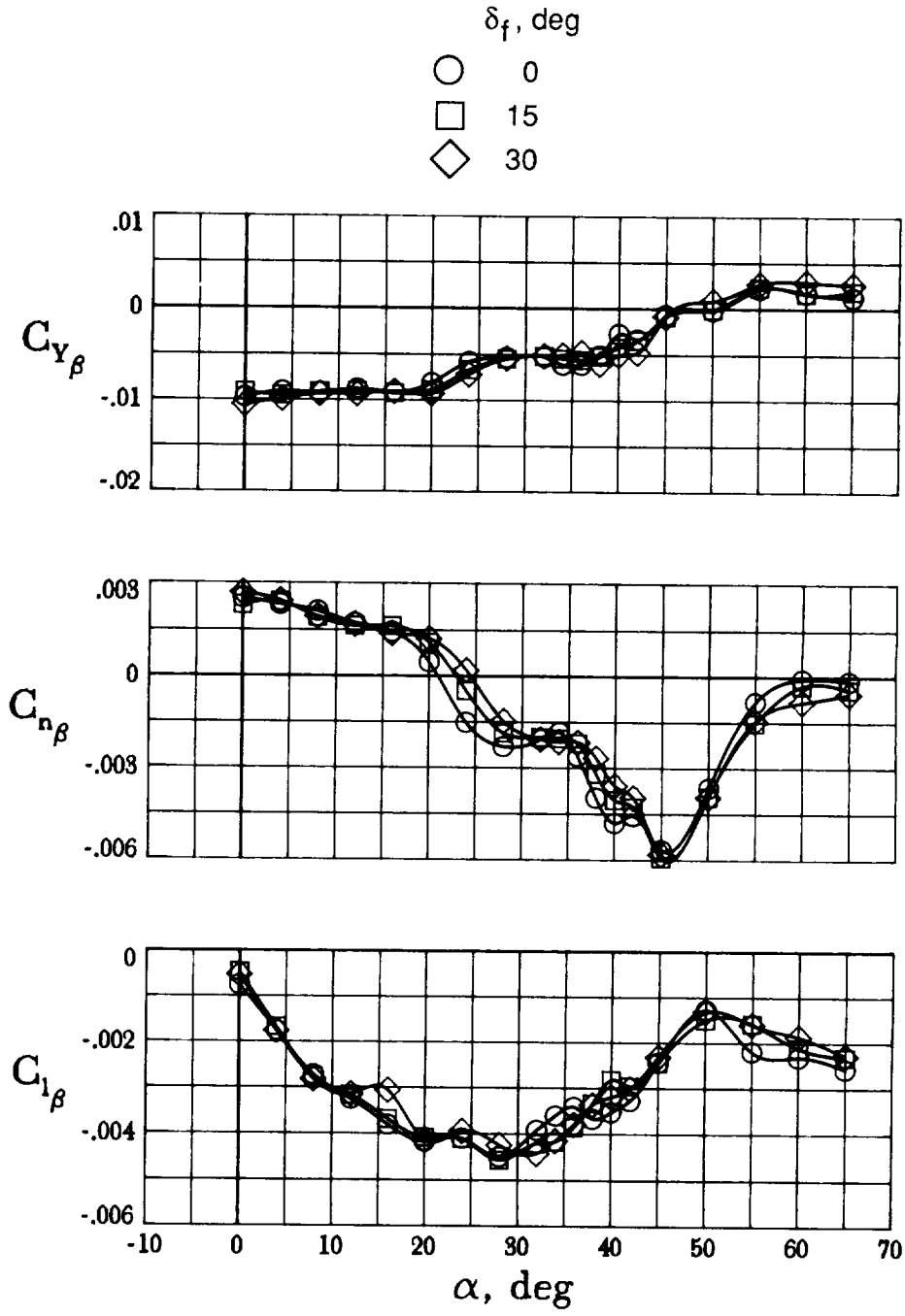

Figure 12. Effect of leading-edge flap deflection on lateral-directional characteristics. $\delta_c = -10°$; $\delta_F = 0°$.

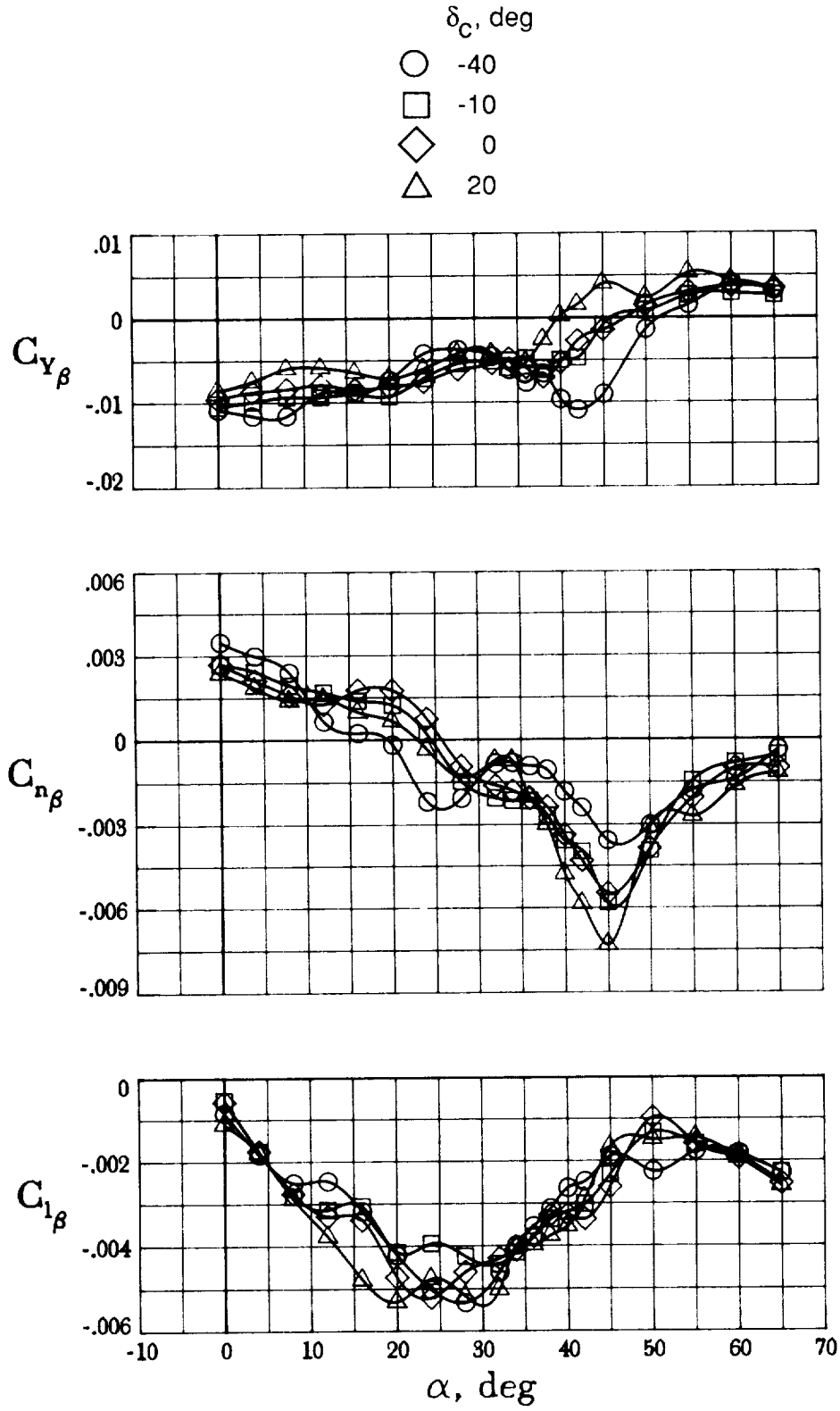

Figure 13. Effect of canard deflection on lateral-directional characteristics. $\delta_f = 30°$; $\delta_F = 0°$.

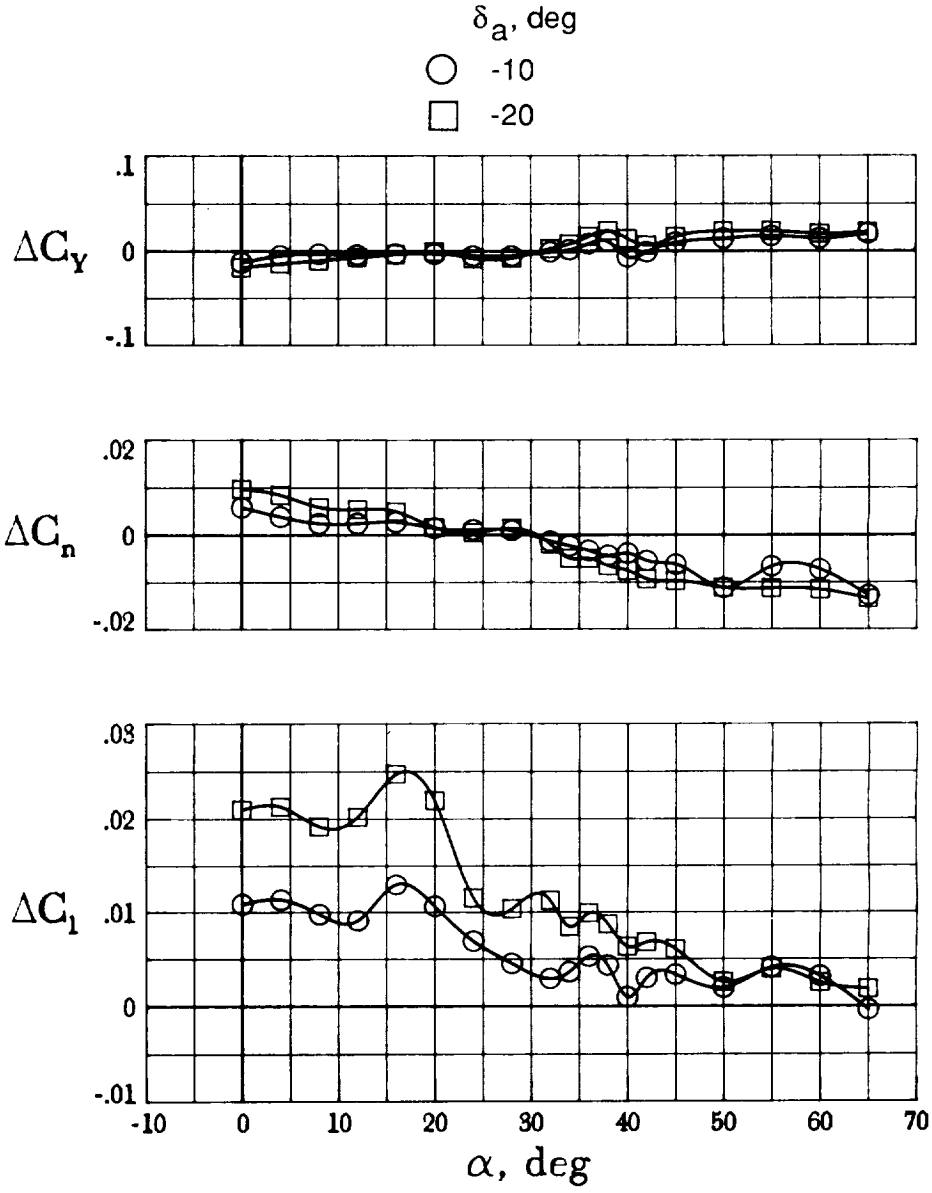

Figure 14. Aileron control effectiveness. $\delta_f = 30°$; $\delta_c = -10°$; $\delta_F = 0°$.

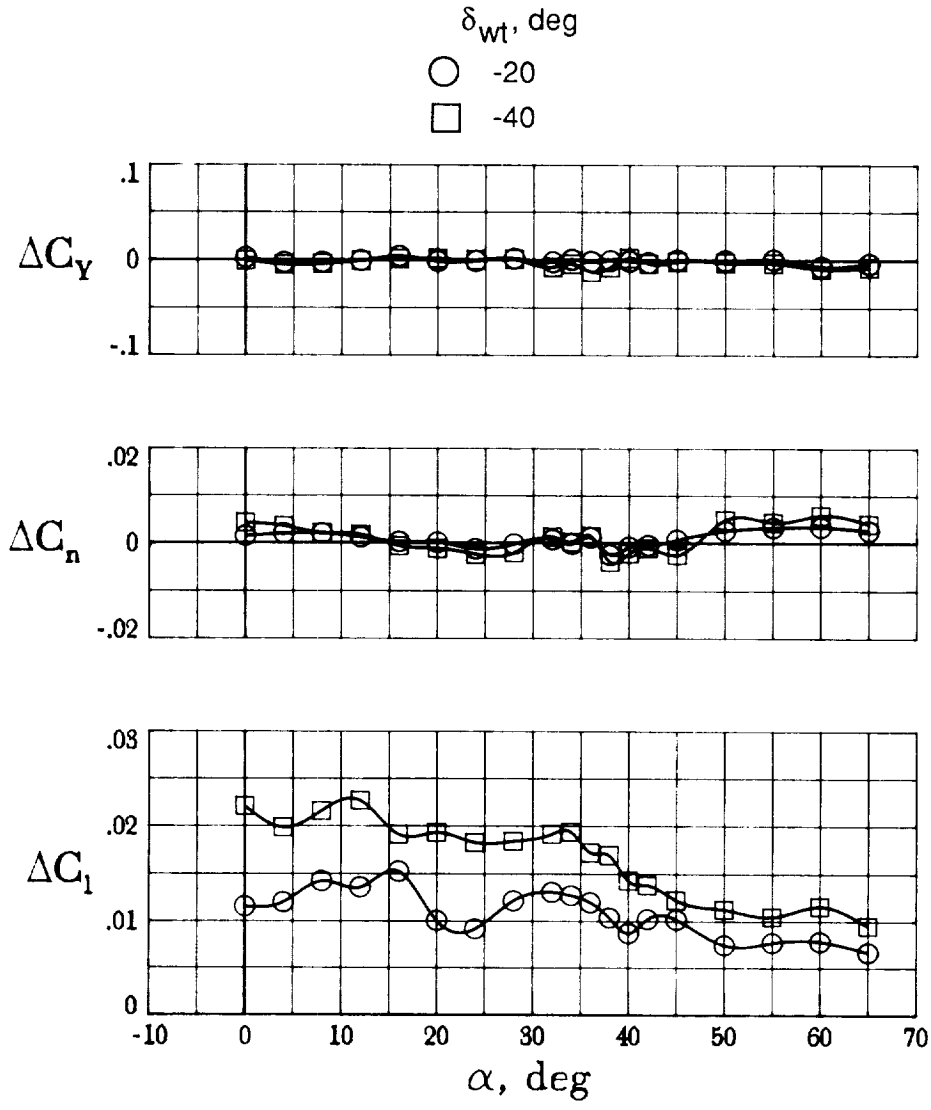

Figure 15. Tiperon control effectiveness. $\delta_f = 30°$; $\delta_c = -10°$; $\delta_F = 0°$.

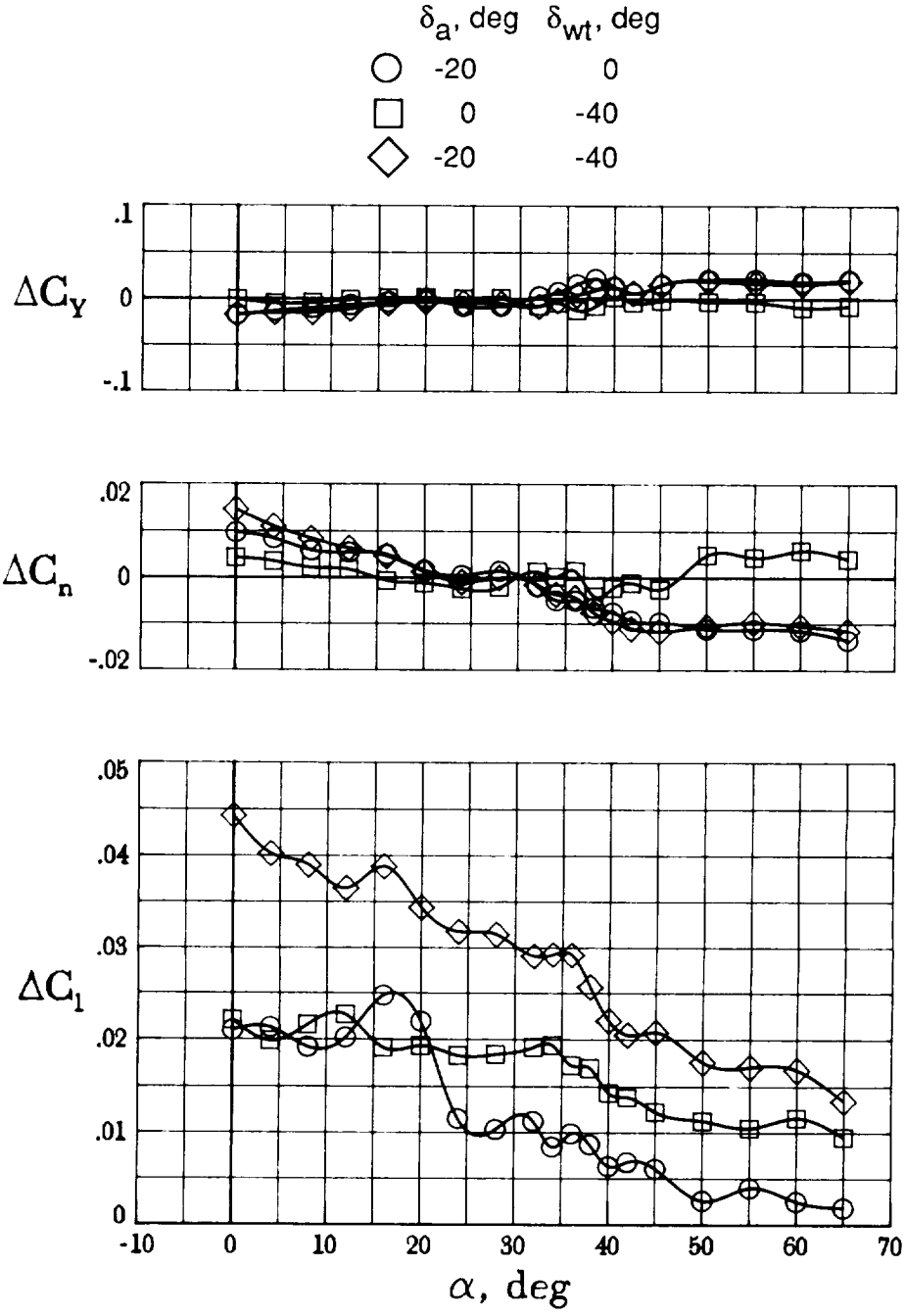

Figure 16. Combined aileron/tiperon control effectiveness. $\delta_f = 30°$; $\delta_c = -10°$; $\delta_F = 0°$.

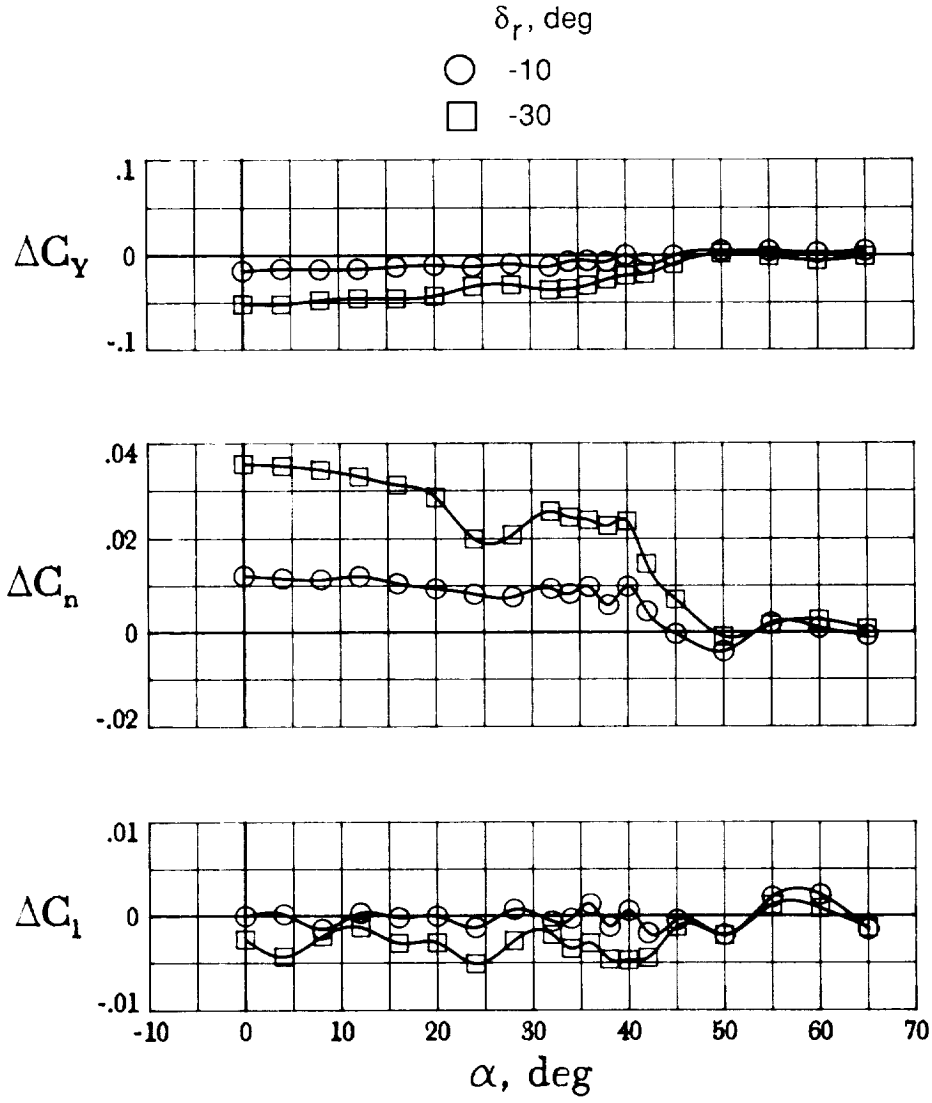

Figure 17. Rudder control effectiveness. $\delta_f = 30°$; $\delta_c = -10°$; $\delta_F = 0°$.

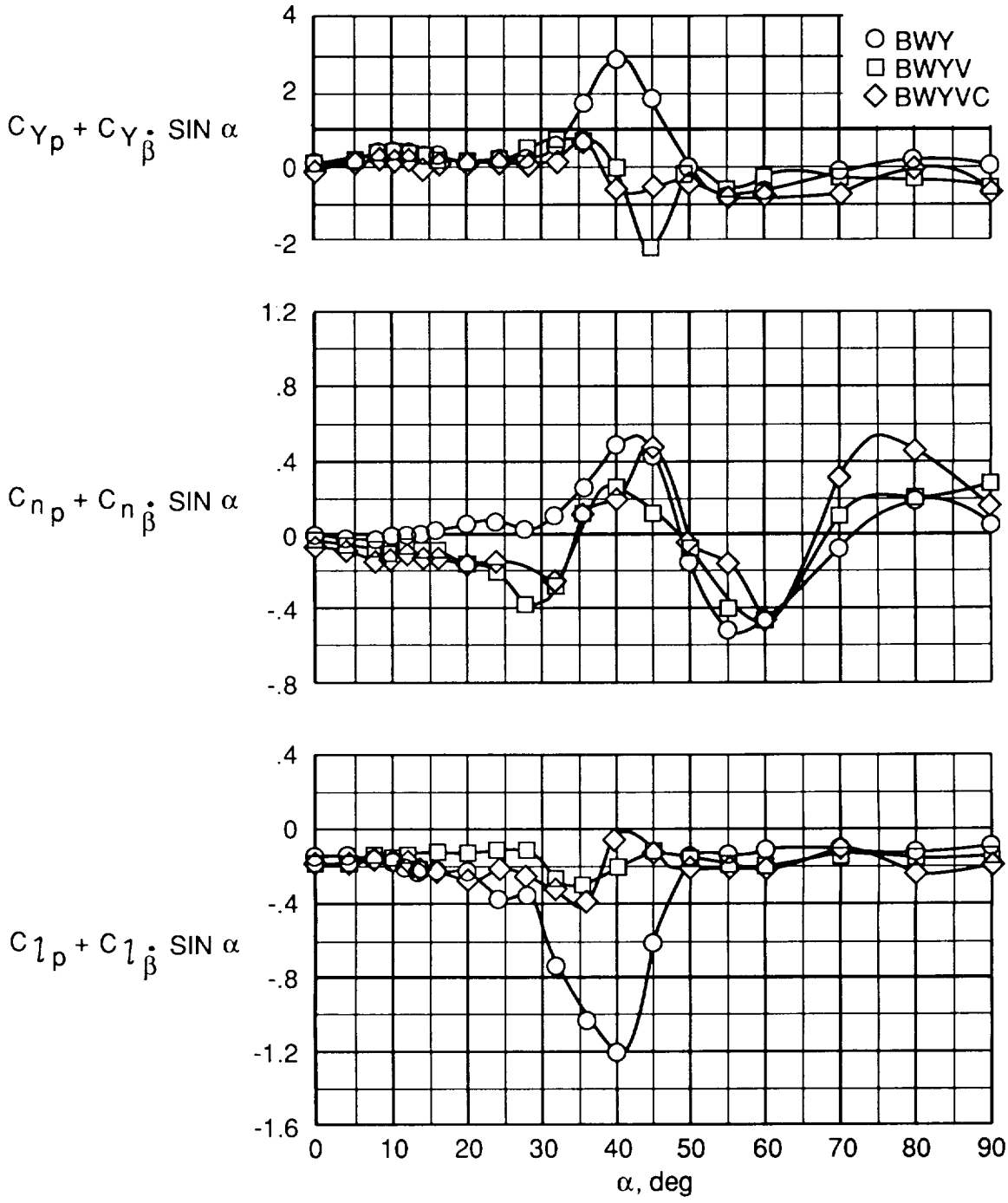

Figure 18. Effect of major geometry component on roll damping. $\delta_f = 30°$; $\delta_c = -10°$; $\delta_F = 0°$.

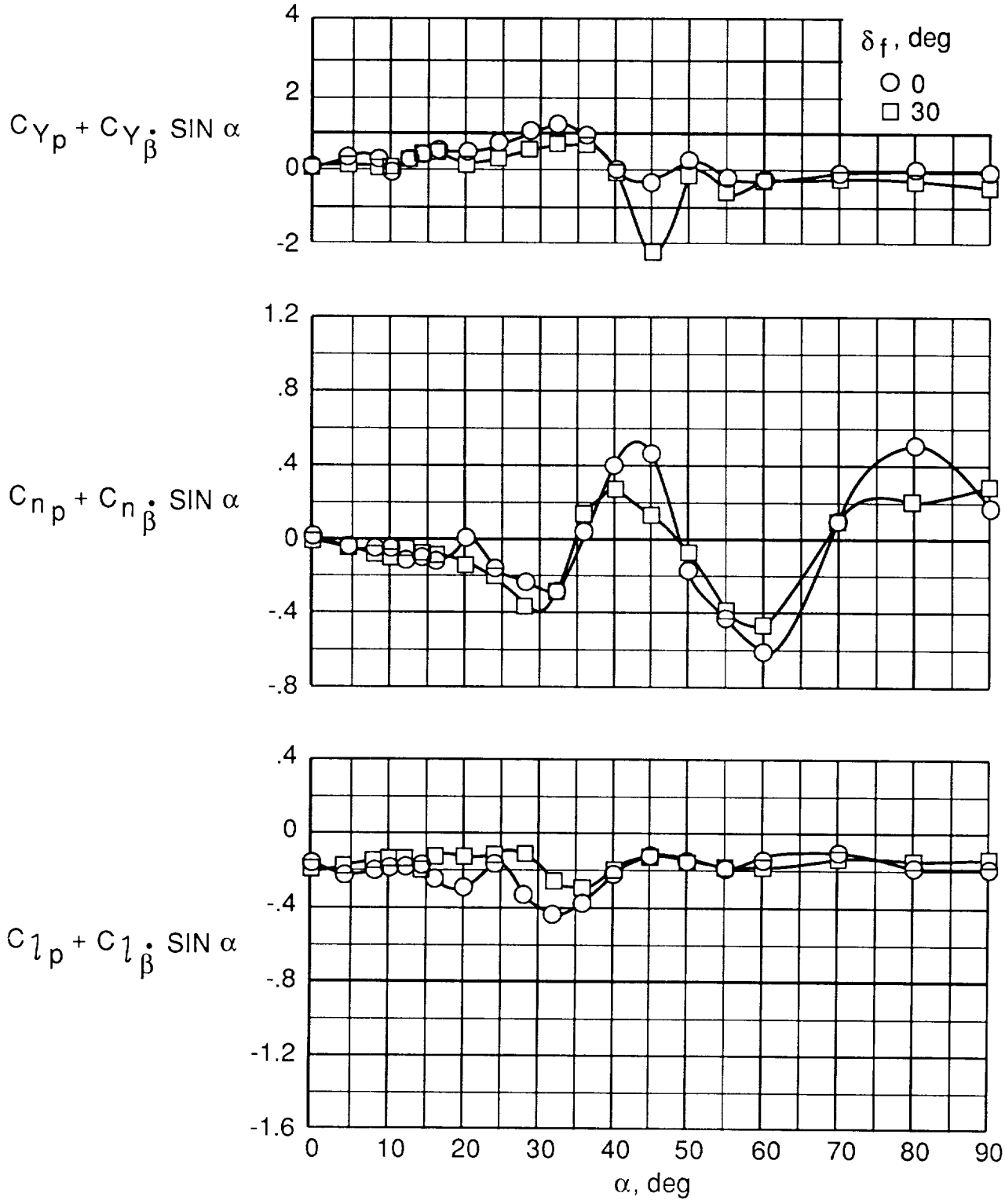

Figure 19. Effect of leading-edge flap deflection on roll damping. Canard off; $\delta_F = 0°$.

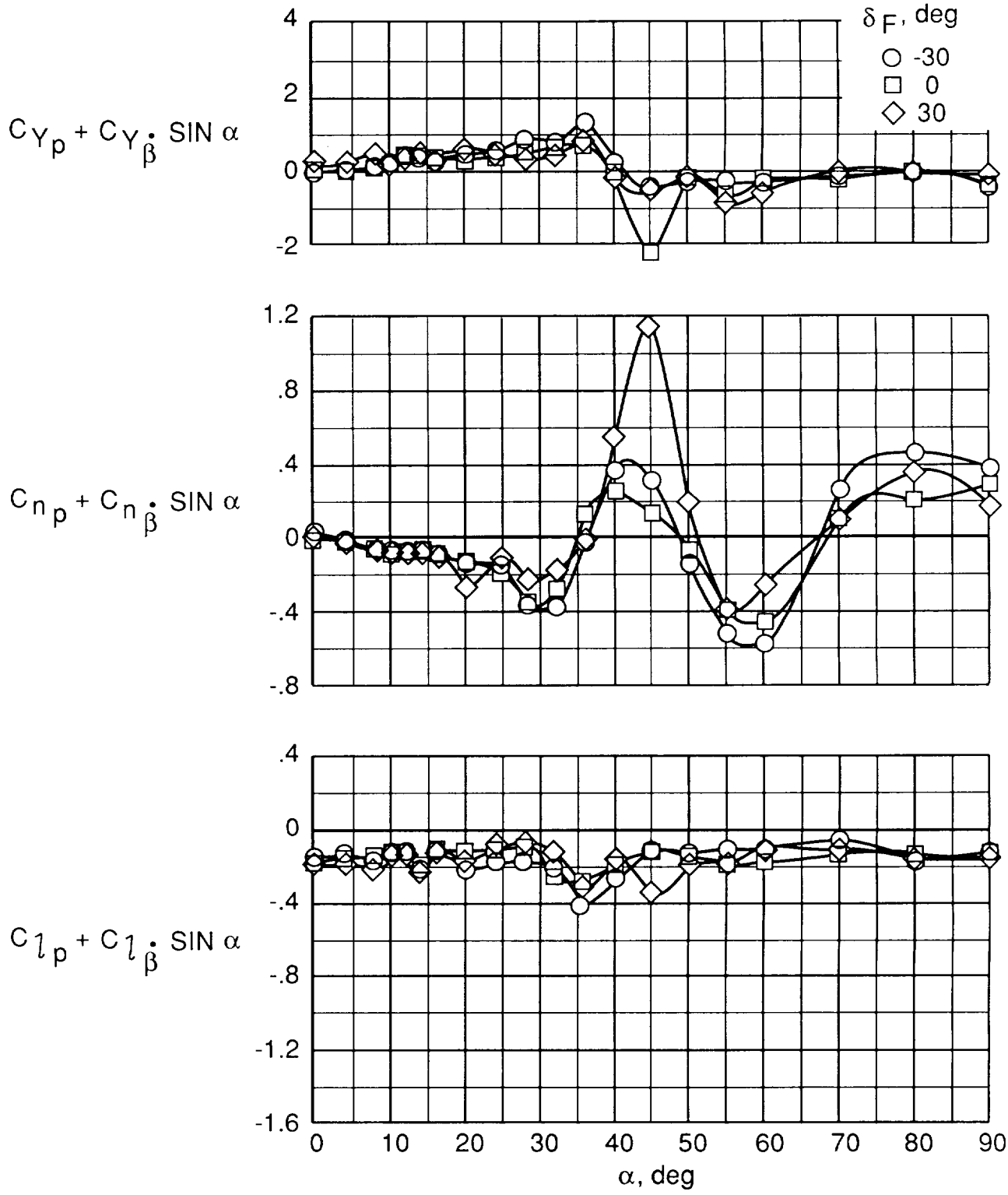

Figure 20. Effect of TEX flap deflection on roll damping. Canard off; $\delta_f = 30°$.

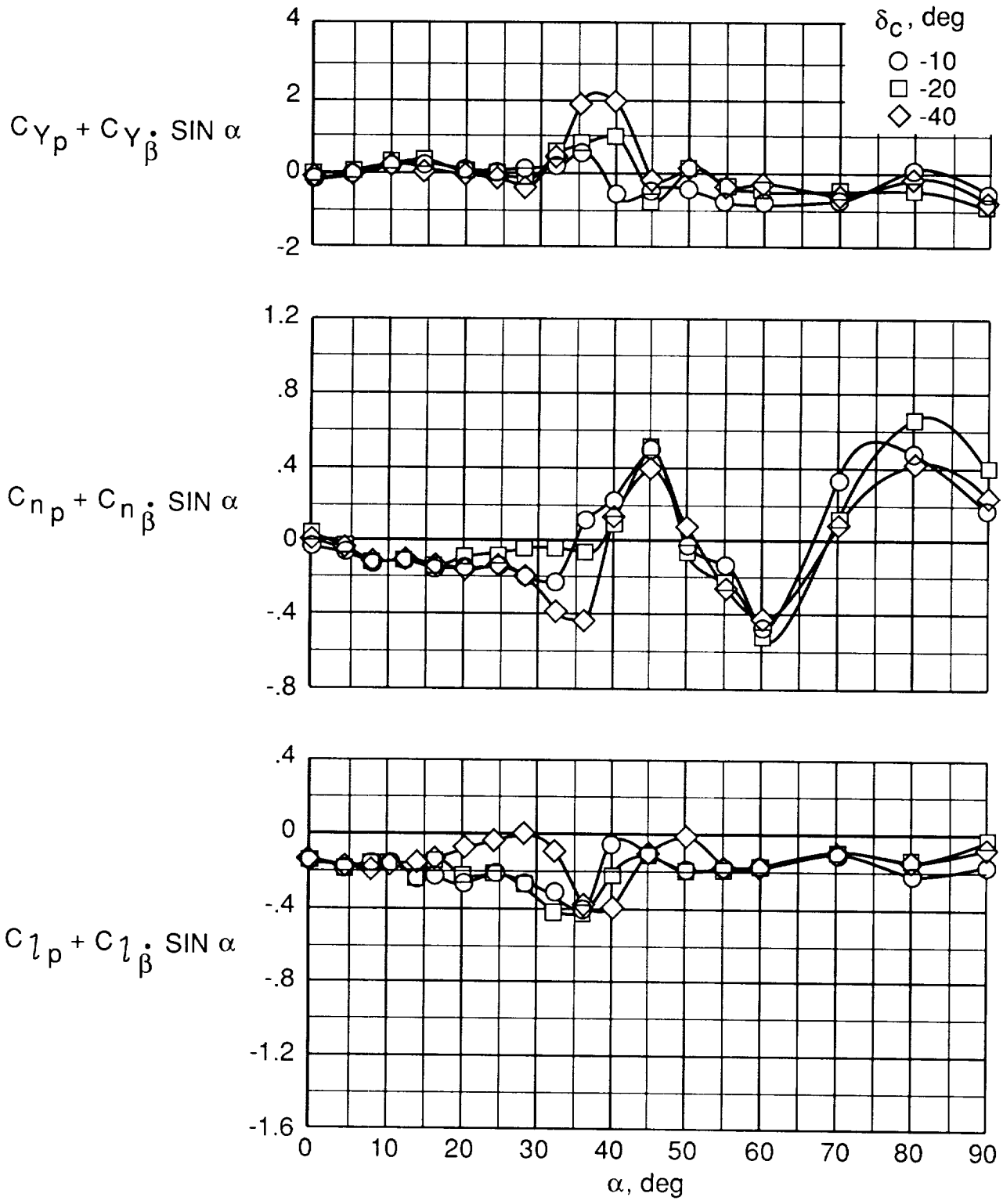

Figure 21. Effect of canard deflection on roll damping. $\delta_f = 30°$; $\delta_F = 0°$.

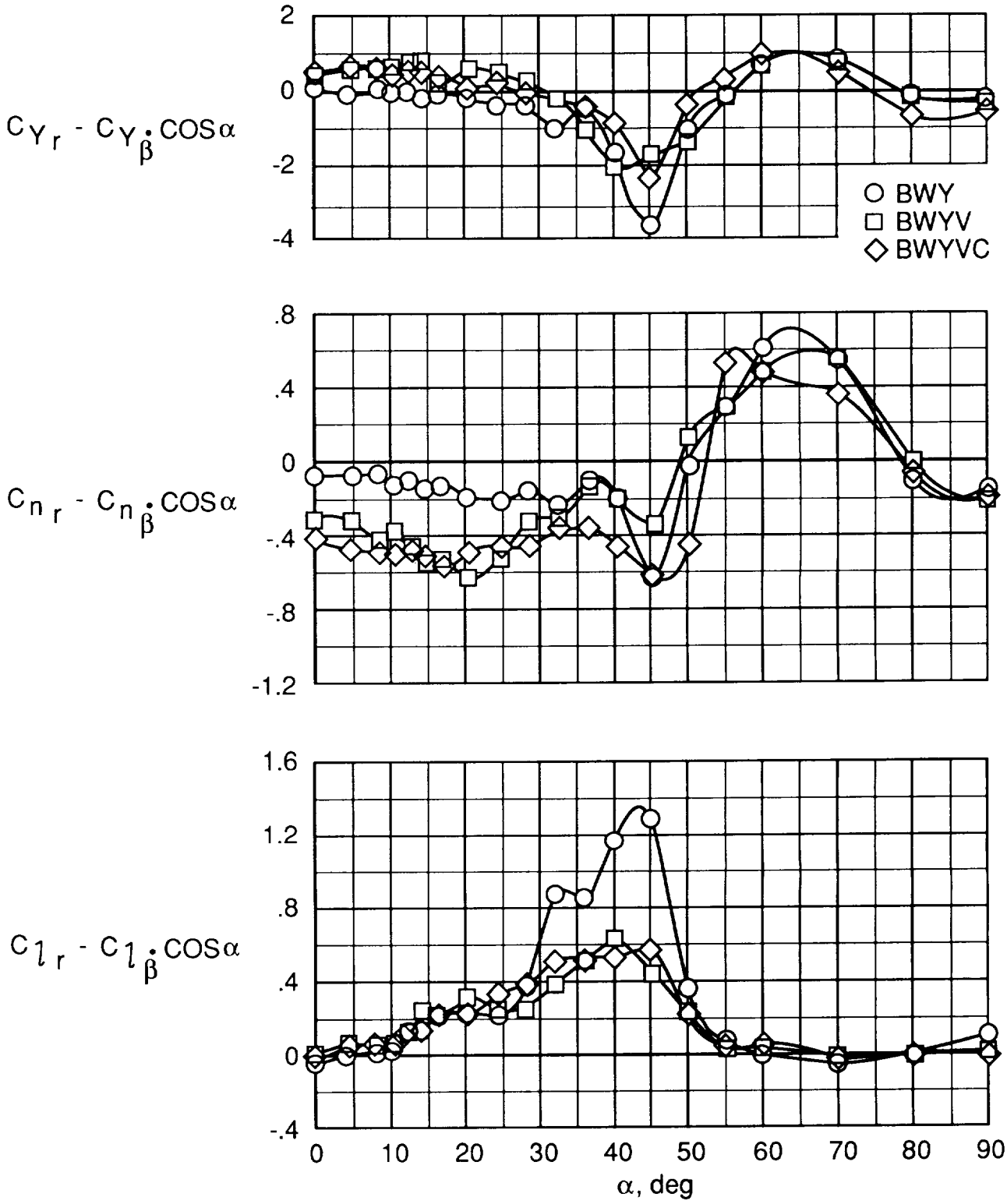

Figure 22. Effect of major geometry component on yaw damping. $\delta_f = 30°$; $\delta_c = -10°$; $\delta_F = 0°$.

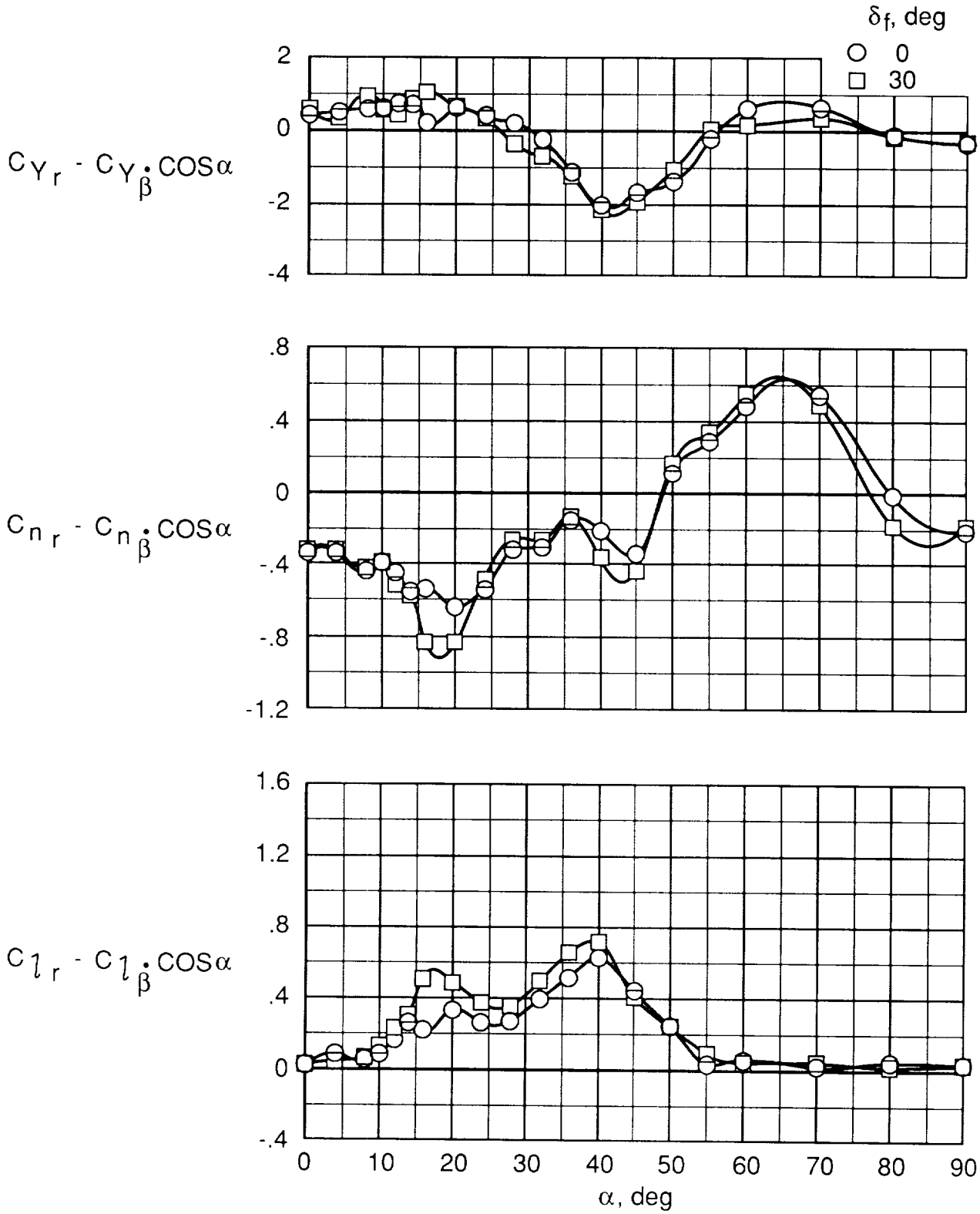

Figure 23. Effect of leading-edge flap deflection on yaw damping. Canard off; $\delta_F = 0°$.

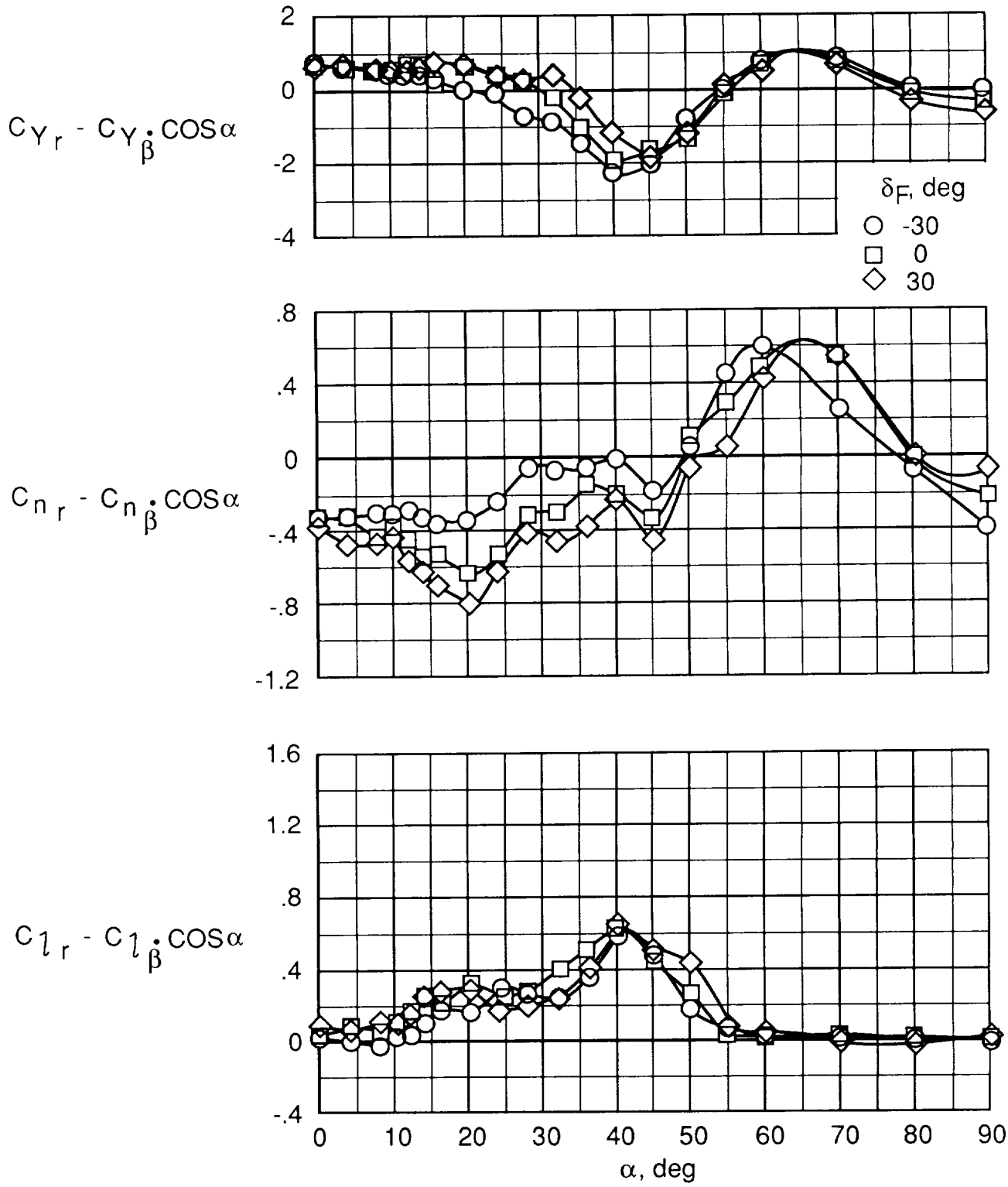

Figure 24. Effect of TEX flap deflection on yaw damping. Canard off; $\delta_f = 30°$.

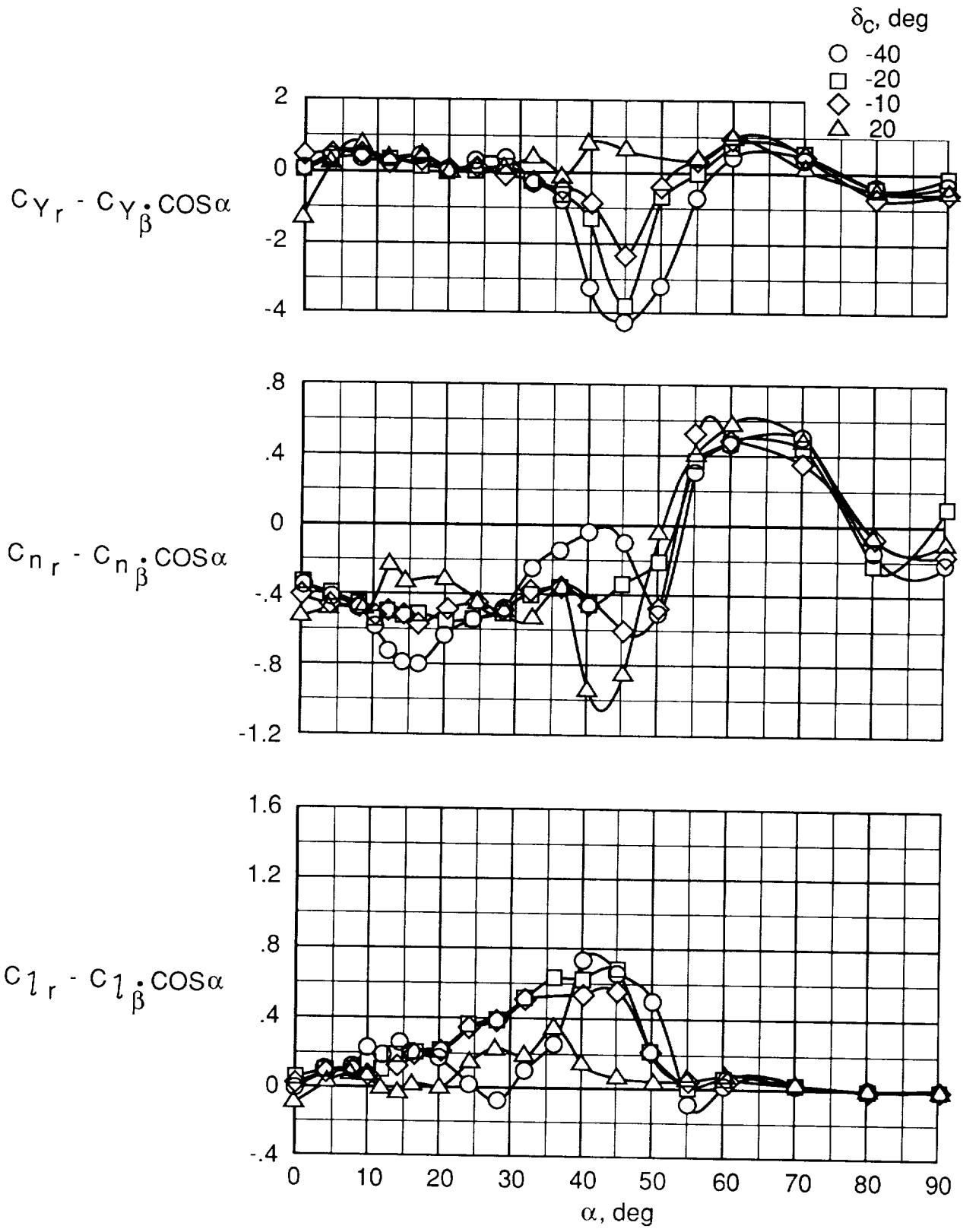

Figure 25. Effect of canard deflection on yaw damping. $\delta_f = 30°$; $\delta_F = 0°$.

NASA
National Aeronautics and Space Administration

Report Documentation Page

1. Report No.	2. Government Accession No.	3. Recipient's Catalog No.
NASA TM-4138		

4. Title and Subtitle	5. Report Date
Low-Speed Static and Dynamic Force Tests of a Generic Supersonic Cruise Fighter Configuration	October 1989
	6. Performing Organization Code
7. Author(s)	8. Performing Organization Report No.
David E. Hahne	L-16599
9. Performing Organization Name and Address	10. Work Unit No.
NASA Langley Research Center Hampton, VA 23665-5225	505-61-71-07
	11. Contract or Grant No.
12. Sponsoring Agency Name and Address	13. Type of Report and Period Covered
National Aeronautics and Space Administration Washington, DC 20546-0001	Technical Memorandum
	14. Sponsoring Agency Code

15. Supplementary Notes

16. Abstract

Static and dynamic force tests of a generic fighter configuration designed for sustained supersonic flight have been conducted in the Langley 30- by 60-Foot Tunnel. The baseline configuration had a 65° arrow wing, twin vertical tails, and a canard. The results of the investigation showed that control was available up to $C_{L,\max}$ (maximum lift coefficient) from aerodynamic controls about all axes, but control in the pitch and yaw angles decreased rapidly in the poststall angle-of-attack region. The baseline configuration showed stable lateral-directional characteristics at low angles of attack but directional stability occurred near an angle of attack of 25° as the wing shielded the vertical tails. The configuration showed positive effective dihedral throughout the test angle-of-attack range. Forced oscillation tests indicated that the baseline configuration had stable damping characteristics about the lateral-directional axes.

17. Key Words (Suggested by Authors(s))	18. Distribution Statement
Stability and control Aerodynamic control concepts Dynamic stability Arrow wing	Unclassified - Unlimited Subject Category 02

19. Security Classif. (of this report)	20. Security Classif. (of this page)	21. No. of Pages	22. Price
Unclassified	Unclassified	33	A03

NASA FORM 1626 OCT 86

NASA-Langley, 1989

For sale by the National Technical Information Service, Springfield, Virginia 22161-2171